

**University of Moratuwa**

**Faculty of Engineering**

**Department of Electronic and Telecommunication  
Engineering**



**EN2160 - Electronic Design Realization**

**Design Report- Strain Gauge based Torque Sensor**

Aashir M.R.M.	220004M
Basith M.N.A.	220071M
Kumarage R.V.	220343B
Manawadu D.N.	220380J
Manawadu M.D.	220381M
Munavvar M.A.A.	220405T
Ransika L.G.C.	220514C
Samuditha H.K.P.	220562U

## Contents

<b>1 Introduction</b>	<b>4</b>
<b>2 Scope and objectives of the project</b>	<b>4</b>
<b>3 Review Progress</b>	<b>5</b>
3.1 Existing Products in the Market . . . . .	5
3.1.1 Various Types of Torque Sensors and Manufacturing Companies . . . . .	5
3.2 Industrial Applications . . . . .	6
<b>4 Theory &amp; Principles</b>	<b>7</b>
4.1 Basic Principle of Torque Measurement via Strain Gauges . . . . .	7
4.2 Strain Gauges . . . . .	7
4.3 Wheatstone Bridge Configuration . . . . .	7
4.4 Relationship Between Torque, Strain, and Output Voltage . . . . .	8
4.4.1 Torque and Shear Stress . . . . .	8
4.4.2 Shear Stress to Strain . . . . .	8
4.4.3 Strain to Voltage . . . . .	8
<b>5 Design Considerations</b>	<b>9</b>
5.1 Mechanical Design . . . . .	9
5.1.1 Overview . . . . .	9
5.1.2 Design Objectives . . . . .	9
5.1.3 Shaft Material Selection . . . . .	9
5.1.4 Shaft Geometry . . . . .	11
5.1.5 Conceptual Designs for Enclosure . . . . .	11
5.1.6 Final Enclosure and Mold Design . . . . .	14
5.1.7 Shaft Placement . . . . .	16
5.1.8 Fabricated Enclosure . . . . .	16
5.1.9 Manufacturing and Assembly . . . . .	17
5.2 Electrical design . . . . .	18
5.2.1 Strain gauge placement and orientation . . . . .	19
5.2.2 Bridge configuration. . . . .	19
5.2.3 Instrumentation Amplifier . . . . .	20
5.2.4 Offset Circuit for Instrumentation Amplifier . . . . .	21
5.2.5 Secondary Amplifier . . . . .	21
5.2.6 Power Supply Requirements and Design . . . . .	22
<b>6 Wireless Power Transmission</b>	<b>23</b>
6.1 Objective . . . . .	23
6.2 Process Flow . . . . .	23
6.3 Coil arrangements . . . . .	23
6.3.1 Environmental Considerations . . . . .	25
<b>7 Component Selection</b>	<b>26</b>
7.1 Strain Gauge . . . . .	26
7.2 Instrumentation Amplifier . . . . .	26
7.3 Offset Circuit for Instrumentation Amplifier . . . . .	27
7.4 Secondary Amplifier . . . . .	28

7.5	Microcontroller Selection . . . . .	28
7.5.1	ADC Integration Strategy Comparison . . . . .	28
7.5.2	MCU Selection Criteria . . . . .	29
7.5.3	Microcontroller Comparison Analysis . . . . .	30
7.5.4	Selected Solution: DA14531 Justification . . . . .	30
<b>8</b>	<b>Schematic Design</b>	<b>31</b>
8.1	Transmitter . . . . .	32
8.2	RECEIVER . . . . .	33
8.3	BOOSTER . . . . .	33
8.4	INSTRUMENTATION . . . . .	34
8.5	OFFSET . . . . .	35
8.6	ADC . . . . .	36
8.7	MCU . . . . .	36
<b>9</b>	<b>PCB DESIGN</b>	<b>37</b>
9.1	Design Considerations . . . . .	37
9.2	Layout Details . . . . .	37
9.3	PCB Specifications . . . . .	38
<b>10</b>	<b>Simulation &amp; Calculations</b>	<b>39</b>
10.1	Finite Element Analysis . . . . .	39
10.2	Enhanced FEA Analysis – Validation of Tensile and Compressive Strain at $\pm 45^\circ$ Orientation . . . . .	40
10.3	Hand Calculations for Expected Strain and Voltage Output with Two Dual-Grid Strain Gauges . . . . .	42
10.3.1	Expected Shear Strain . . . . .	42
10.3.2	Normal Strain for Strain Gauges . . . . .	42
10.3.3	Voltage Output from Full Wheatstone Bridge . . . . .	42
<b>11</b>	<b>Sensitivity analysis</b>	<b>43</b>
<b>12</b>	<b>Microcontroller Programming and Communication Setup</b>	<b>44</b>
12.1	GPIO Reservation and Pad Configuration . . . . .	45
12.2	HX711 Data Acquisition and BLE Transmission . . . . .	46
<b>13</b>	<b>Design Revisions and Improvements</b>	<b>47</b>
13.1	Instrumentation amplifier . . . . .	47
13.2	Secondary Amplifier . . . . .	48
13.3	Offset Circuit for Instrumentation — Switching to OPA336 for instrumentation amplifier . . . . .	48
13.4	Fabricated Enclosure . . . . .	48
13.5	Transmitter PCB . . . . .	49
<b>14</b>	<b>Bill of materials and cost analysis</b>	<b>50</b>
<b>15</b>	<b>Conclusion</b>	<b>50</b>
<b>16</b>	<b>References</b>	<b>51</b>

# 1 Introduction

Torque measurement plays a crucial role in mechanical systems where rotational forces are involved, such as motors, gearboxes, and power transmission assemblies. Accurate torque sensing enables performance monitoring, process control, and preventive maintenance across a wide range of industrial applications.

This design report presents the development of a strain gauge-based torque sensor intended to meet industrial standards for accuracy, reliability, and robustness. The project involves the design, fabrication, and testing of a torque measurement system based on the mechanical deformation of a rotating shaft under torsional load. The strain induced in the shaft is captured using precision strain gauges arranged in a full Wheatstone bridge configuration to maximize sensitivity.

The report covers the theoretical background of torque sensing, the design principles used in both the mechanical and electrical subsystems and validation results. Emphasis has been placed on creating a cost-effective yet high-performance solution suitable for real-world industrial environments.

By the end of this report, the reader will gain a comprehensive understanding of the design approach, component selection, system integration, and testing methodology employed in the realization of the torque sensor.

## 2 Scope and objectives of the project

The scope of this project is to design and develop a strain gauge-based torque sensor that meets industrial standards for accuracy, reliability, and durability. The measurement range of the torque sensor is 50Ncm. It should be used wireless method to transmit the power and signal between rotor and stator. The sensor is intended for use in real-world mechanical systems.

**The primary objectives of the project are:**

- To investigate the mechanical and electrical principles behind torque measurement using strain gauges.
- To design a robust and mechanically sound shaft structure suitable for torque transmission and strain gauge integration.
- To implement a full-bridge Wheatstone circuit configuration for high sensitivity and thermal compensation.
- To design and integrate signal conditioning circuitry that amplifies and filters the strain signal for stable and accurate readings.
- To ensure the sensor design adheres to key industrial criteria such as repeatability, linearity, stability, and environmental resilience.
- To document the full design and development process with consideration for scalability, manufacturing.

This project aims to deliver a torque sensor that not only demonstrates strong technical fundamentals but is also built to withstand the demands of industrial applications.

### 3 Review Progress

This section presents a review of existing torque sensor technologies, leading manufacturers in the market, and the typical industrial applications where these sensors are deployed. Understanding the current state of the art provides valuable context and benchmarking criteria for the design and implementation of our own torque sensor.

#### 3.1 Existing Products in the Market

A wide range of torque sensors is currently available in the global market, catering to various applications from automotive and aerospace to robotics and heavy industry. These products differ in terms of measurement principle, range, size, accuracy, and environmental resistance. Many high-end torque sensors offer features such as digital interfaces, temperature compensation, overload protection, and wireless telemetry.

##### 3.1.1 Various Types of Torque Sensors and Manufacturing Companies

Torque sensors can be categorized based on their working principles. Some of the most common types include:

- **Strain Gauge-Based Torque Sensors:** These are the most widely used type, employing bonded strain gauges on a rotating shaft. They offer high accuracy and are relatively easy to integrate.
- **Magnetoelastic Torque Sensors:** These operate based on changes in magnetic properties of a material under strain. They are robust and suitable for harsh environments.
- **Optical Torque Sensors:** These utilize laser-based or optical encoding techniques to measure angular displacement and resulting torque. They provide high resolution and are used in precise laboratory settings.
- **Surface Acoustic Wave (SAW) Sensors:** These are non-contact, wireless sensors that use SAW technology to detect strain. They are increasingly adopted in advanced industrial systems.
- **Rotary and Reaction Torque Sensors:** Rotary sensors measure dynamic torque on rotating systems, while reaction torque sensors measure static or slowly varying torque in fixed systems.

Some of the leading companies manufacturing torque sensors include:

- **LORD Sensing Microstrain** - is another prominent manufacturer specializing in torque sensors, particularly known for its advanced sensing solutions for harsh environments.
- **HBM (Hottinger Brüel & Kjær)** – Offers a broad portfolio of strain gauge-based sensors with excellent precision.
- **Futek Advanced Sensor Technology** – Specializes in miniature and custom torque sensors for aerospace and medical applications.
- **Kistler Group** – Known for high-performance torque sensors used in powertrain testing and industrial automation.
- **Interface Inc.** – Produces a wide variety of rotary and reaction torque transducers with calibration services.

These products typically come with calibration certificates, long operational lifespans, and advanced digital interfaces (e.g., CAN, RS-485, USB) to suit modern automation systems.

### 3.2 Industrial Applications

Torque sensors play a vital role in modern industrial systems. Their primary function is to measure the rotational force applied to shafts, spindles, or rotating equipment, enabling closed-loop control and monitoring.

Key industrial applications include:

- **Automotive Industry:** Used in engine testing, transmission development, electric vehicle drive systems, and powertrain efficiency analysis.
- **Robotics:** Integrated into robotic joints and grippers for force feedback and motion control, enabling tasks such as delicate assembly or collaborative human-robot interaction.
- **Industrial Automation:** Employed in assembly lines to control tightening torques, monitor motor loads, and ensure consistent product quality.
- **Aerospace:** Used for component testing, actuator feedback systems, and simulation rigs.
- **Energy Sector:** Utilized in wind turbine monitoring, hydraulic systems, and testing of rotating generators and motors.
- **Medical Devices:** Miniature torque sensors are found in surgical robots and prosthetics to ensure precise control and user feedback.

As industries evolve toward smart and connected systems (Industry 4.0), the demand for torque sensors with enhanced digital capabilities, remote monitoring, and predictive maintenance features continues to grow.



Figure 1: Torque sensor used in Robot arms



Figure 2: Torque sensor shaft

## 4 Theory & Principles

### 4.1 Basic Principle of Torque Measurement via Strain Gauges

Torque measurement using strain gauges relies on the relationship between applied torque and the resulting shear strain in a rotating shaft. When torque is applied, the shaft undergoes torsional deformation, causing shear strain on its surface. Strain gauges bonded at specific orientations on the shaft surface convert this mechanical deformation into a measurable change in electrical resistance. By analyzing this change, the applied torque can be determined.

### 4.2 Strain Gauges

A **strain gauge** is a sensor that changes its electrical resistance when subjected to strain. It typically consists of a metallic foil grid bonded to a surface. As the surface deforms, the gauge experiences a change in length and diameter, leading to a change in resistance.

**Gauge Factor (GF)** is a key parameter that defines the sensitivity of the strain gauge:

$$GF = \frac{\Delta R/R}{\varepsilon}$$

where:

- $\Delta R$  is the change in resistance,
- $R$  is the original resistance,
- $\varepsilon$  is the strain.

For torque measurements, strain gauges are typically mounted at  $\pm 45^\circ$  angles relative to the shaft axis to capture shear strain effectively.

### 4.3 Wheatstone Bridge Configuration

Because strain-induced resistance changes are very small, a **Wheatstone bridge** circuit is used to detect them precisely. It consists of four resistors arranged in a diamond configuration. Based on the number of active strain gauges, the bridge can be:

- **Quarter-bridge:** One active strain gauge.
- **Half-bridge:** Two active strain gauges (in tension and compression).
- **Full-bridge:** Four active strain gauges (maximum sensitivity and temperature compensation).

The output voltage of a quarter-bridge configuration is approximately:

$$V_{\text{out}} = \left( \frac{\Delta R}{R} \right) \cdot \left( \frac{V_{\text{exc}}}{4} \right)$$

where  $V_{\text{exc}}$  is the excitation voltage applied to the bridge.

In this project, we selected the **full-bridge configuration** for strain gauge measurements.

The full-bridge consists of four active strain gauges arranged such that two gauges are placed in areas under tensile strain and two in areas under compressive strain. This configuration offers several advantages:

- **Maximum sensitivity:** All four gauges contribute to the output signal, effectively quadrupling the signal strength compared to a quarter-bridge.
- **Temperature compensation:** Since all gauges experience the same environmental conditions, any temperature-induced resistance changes are cancelled out.
- **Improved signal-to-noise ratio:** The amplified differential output from a full bridge is less susceptible to noise and interference.

Due to these benefits, especially the improved accuracy and thermal stability, the full-bridge configuration was deemed the most suitable for our torque sensor application.

## 4.4 Relationship Between Torque, Strain, and Output Voltage

### 4.4.1 Torque and Shear Stress

$$\tau = \frac{T \cdot r}{J}$$

where:

- $\tau$  is the shear stress,
- $T$  is the applied torque,
- $r$  is the outer radius of the shaft,
- $J$  is the polar moment of inertia.

For a hollow circular shaft,  $J$  is given by:

$$J = \frac{\pi}{2} \cdot (r_o^4 - r_i^4)$$

### 4.4.2 Shear Stress to Strain

$$\gamma = \frac{\tau}{G}$$

where  $G$  is the shear modulus of the shaft material.

### 4.4.3 Strain to Voltage

The strain  $\varepsilon$  alters the resistance of the strain gauge, which in turn changes the output voltage of the Wheatstone bridge. This voltage is proportional to the applied torque, enabling accurate real-time measurement.

## 5 Design Considerations

### 5.1 Mechanical Design

#### 5.1.1 Overview

The mechanical design of the strain gauge torque sensor centers around a solid cylindrical shaft enclosed within a protective housing. Torque is applied to the shaft via its two exposed ends, while the middle section remains inside a sealed enclosure that contains all sensing and signal conditioning components. Strain gauges are mounted on the end region of the shaft to measure the strain induced by applied torque.

#### 5.1.2 Design Objectives

The primary mechanical design goals for the strain gauge torque sensor are:

- **Enable Accurate Torque Transmission and Measurement:** Design the shaft and strain gauge mounting area to ensure measurable and reliable strain under applied torsion.
- **Ensure Structural Integrity and Safety:** Select materials and dimensions that prevent failure or permanent deformation under expected torque loads, with a sufficient safety factor.
- **Protect Internal Components with a Robust Enclosure:** Create a sealed housing that shields the strain gauges, wiring, and electronics from environmental exposure, while allowing shaft rotation at both ends.
- **Support Long-Term Fatigue Resistance:** Design for durability under cyclic loading conditions, using appropriate materials and geometry to avoid fatigue failure over time.
- **Facilitate Easy Manufacturing and Assembly:** Use standard, machinable parts and simple joining methods for ease of fabrication, gauge installation, and maintenance.

#### 5.1.3 Shaft Material Selection

**Selection Methodology** Material selection followed a systematic approach using decision matrices and property analysis. The primary evaluation criteria included mechanical properties, cost, machinability, and suitability for strain gauge application.

**Detailed Material Comparative Analysis** Three commonly used materials in the industry were thoroughly evaluated to determine which would best suit our product.

Feature	AISI 1018 (Low Carbon Steel)	AISI 1045 (Medium Carbon Steel)	AISI 4340NMMO (Medium Alloy Steel)
Yield Strength	~370 MPa	~450 MPa	~400-450 MPa
Tensile Strength	~440 MPa	~620 MPa	~600-700 MPa
Elastic Modulus	~200 GPa	~200 GPa	~200 GPa
Machinability	Excellent	Good	Good
Weldability	Excellent	Moderate	-
Best Application	Small, precise torque sensors	Slightly higher torque applications	Rugged torque sensors
Torque Range Suitability	Ideal for 0-5 N·m, 5 N·m limit	-	Ideal for 0-5 N·m, 10 N·m with null limit

Table 1: Material Comparison for Torque Sensor Shaft

**Selected Material: AISI 1018 Low Carbon Steel** AISI 1018 was selected for the torque sensor shaft based on detailed analysis of:

### Mechanical Properties

- Yield strength of 370 MPa provides sufficient elastic range for the intended torque measurements
- Tensile strength of 440 MPa ensures structural integrity
- Elastic modulus of 200 GPa offers predictable strain response
- High linearity in the elastic region ensures measurement accuracy

### Manufacturing Considerations

- Superior machinability rating ensures precise shaft manufacturing
- Excellent surface finish potential improves strain gauge bonding
- Good dimensional stability after machining minimizes calibration drift
- Cost-effective compared to alloy alternatives, supporting project budget constraints

Although AISI 1018 was selected based on the aforementioned factors, further research and finite element analysis (FEA) were conducted to validate its suitability and explore the potential of alternative materials.

**Industry Recommendation and Market Constraint** The industry-recommended material was AISI 2024, an aluminum alloy containing approximately 70% aluminum, known for its excellent strength-to-weight ratio and good fatigue resistance. However, due to market unavailability of AISI 2024, the team opted for Aluminum 6061 as an alternative.

**Revised Material Selection: Aluminum 6061** While Aluminum 6061 offers lower strength compared to AISI 2024 and the earlier considered steels, it remains a practical option under constrained sourcing conditions. The key considerations for selecting Aluminum 6061 included:

- Adequate mechanical properties for moderate torque loads.

- Significantly lower weight, facilitating easier rotation and less inertia.
- Good machinability and corrosion resistance.
- Increased deformation under torque improves strain gauge resolution, although requiring careful calibration due to lower stiffness.

In conclusion, the final material selection was a result of a combination of technical evaluation, simulation-based validation, industry input, and real-world availability. Aluminum 6061, while not the top recommendation, offered a viable and manufacturable solution aligned with the project's goals.

#### 5.1.4 Shaft Geometry

##### Shaft Diameter Calculation

Using the torsion formula,

$$T_{max} = \frac{J T_{max}}{r}$$

$$T_{max} = \left( \frac{\pi d^4}{32} \right) \frac{T_{max}}{r}$$

$T_{max}$  of AISI 1018 = 272.8

$$1 \text{ Nm} = \frac{\pi}{32} \times \left( \frac{r}{2} \right)^4 \times \frac{272.8 \times 10^6}{r}$$

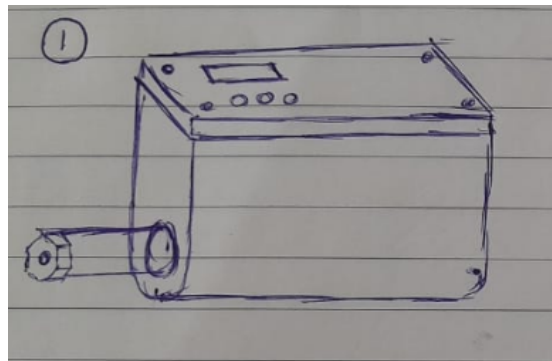
$$r = 8.5 \text{ mm}$$

Figure 3: Shaft Diameter

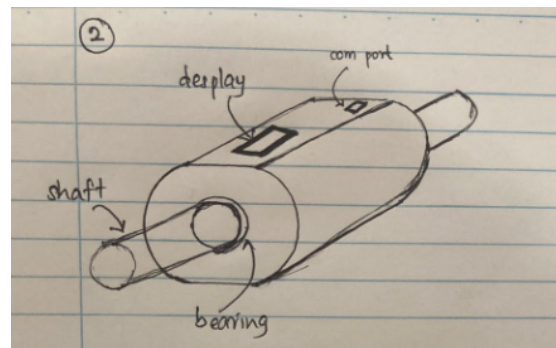
Through this analysis and consideration of safety factors, the optimal shaft diameter was determined to be 17 mm (radius 8.5 mm).

#### 5.1.5 Conceptual Designs for Enclosure

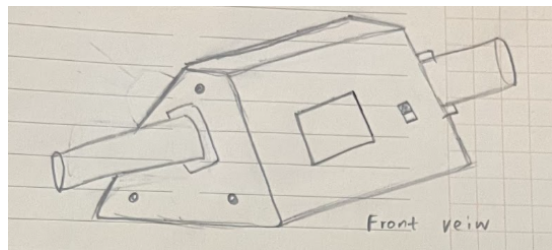
Several conceptual designs were explored to optimize the Shaft's geometry and functionality. These concepts focused on ensuring proper mounting, accessibility for measurement devices, and compatibility with torsional loading.



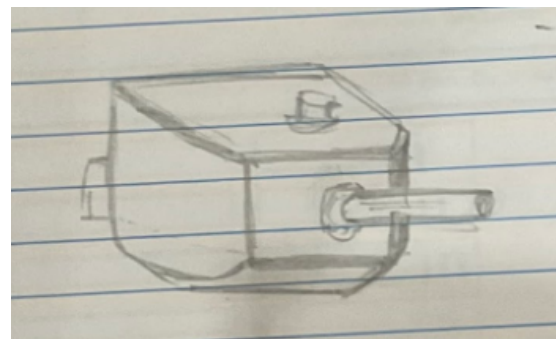
(a) Conceptual Design 1



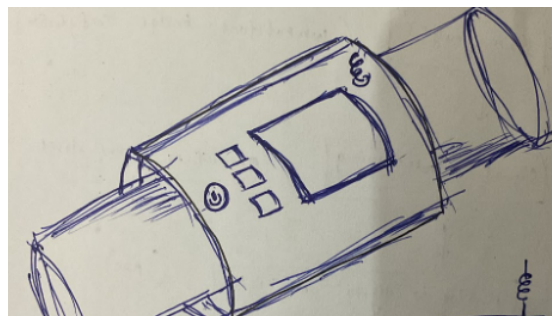
(b) Conceptual Design 2



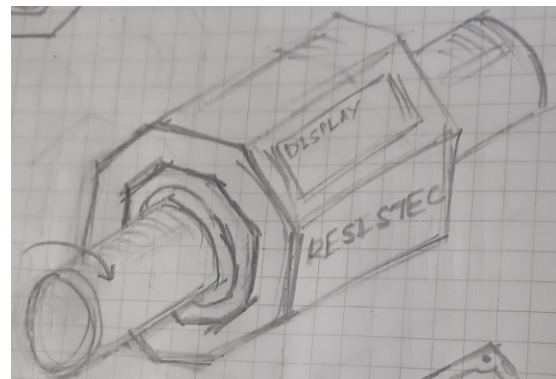
(a) Conceptual Design 3



(b) Conceptual Design 4



(a) Conceptual Design 5



(b) Conceptual Design 6

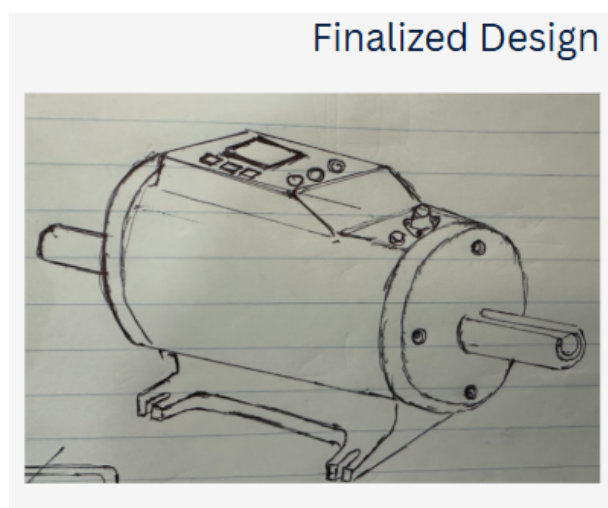


Figure 7: Conceptual design 7

**Design Evaluation Matrix** The seven design concepts were evaluated using a weighted scoring system:

Design Criteria	1	2	3	4	5	6	7
Ergonomics	5	7	6	6	6	7	9
Aesthetic	6	7	6	7	7	8	8
Durability & Robustness	6	6	6	7	7	7	7
Display Feature	7	7	7	7	7	7	7
Communication Port	10	10	10	10	10	10	10
Rechargeability	10	10	10	10	10	10	10
Manufacturability	7	8	7	9	8	7	8
Cost Effectiveness	8	8	7	8	8	8	8
<b>Total Score</b>	<b>59</b>	<b>63</b>	<b>59</b>	<b>64</b>	<b>63</b>	<b>64</b>	<b>67</b>

Table 2: Design Evaluation Matrix for Torque Sensor Concepts

Design 7 was selected as the optimal solution based on its superior performance across all evaluation criteria, particularly:

1. **Superior Ergonomics (Score 9):** The cylindrical form with integrated grips and optimized weight distribution earned the highest ergonomics score, making it significantly more comfortable for laboratory use.
2. **Excellent Aesthetics (Score 8):** The professional appearance with balanced proportions and clean lines provides a high-quality presentation suitable for laboratory equipment.
3. **Strong Manufacturability (Score 8):** The design incorporates manufacturing-friendly features including appropriate draft angles, minimal undercuts, and strategic parting lines.
4. **Compliance with Mechanical Requirements:** Design 7 best accommodated all structural, environmental, interface, manufacturing requirements while maintaining usability.
5. **Alignment with Design Objectives:** Most importantly, Design 7 best fulfilled all five key design objectives, providing the optimal platform for the strain-based torque sensing system.

### 5.1.6 Final Enclosure and Mold Design

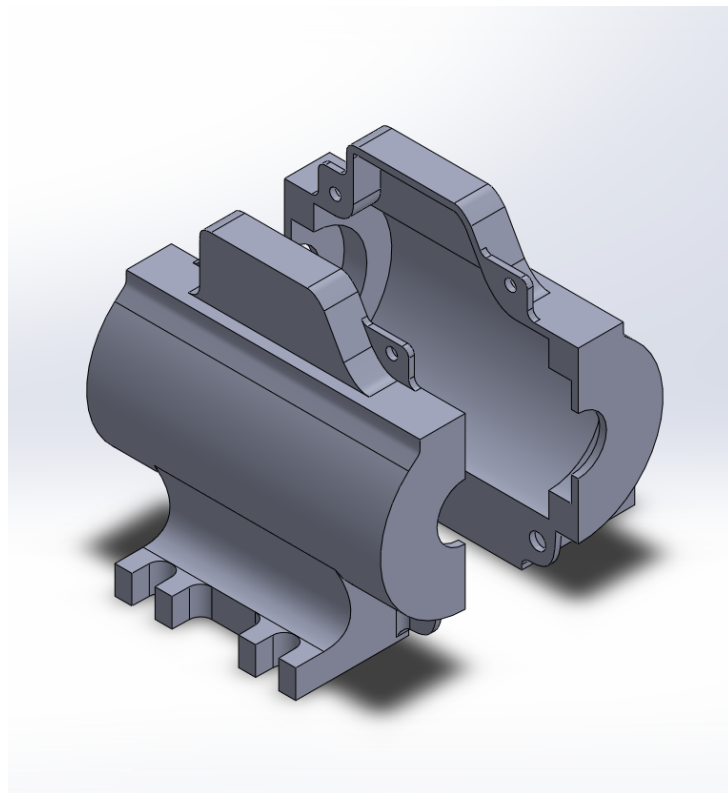


Figure 8: Enclosure

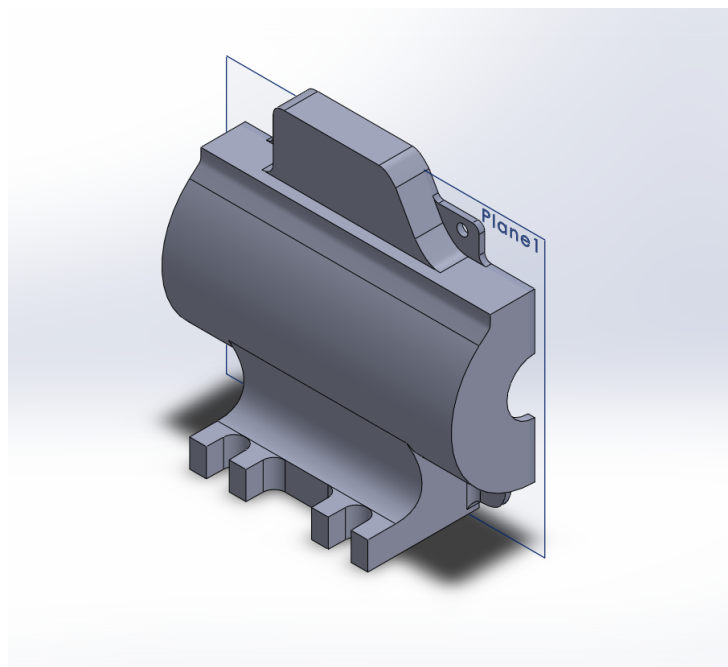


Figure 9: half 1 - isometric

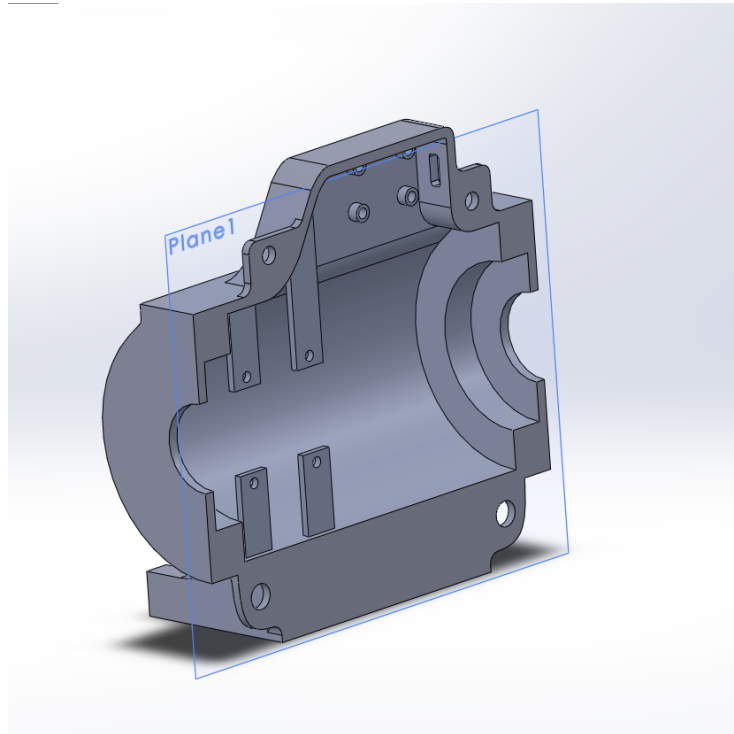


Figure 10: half 1 - inside view

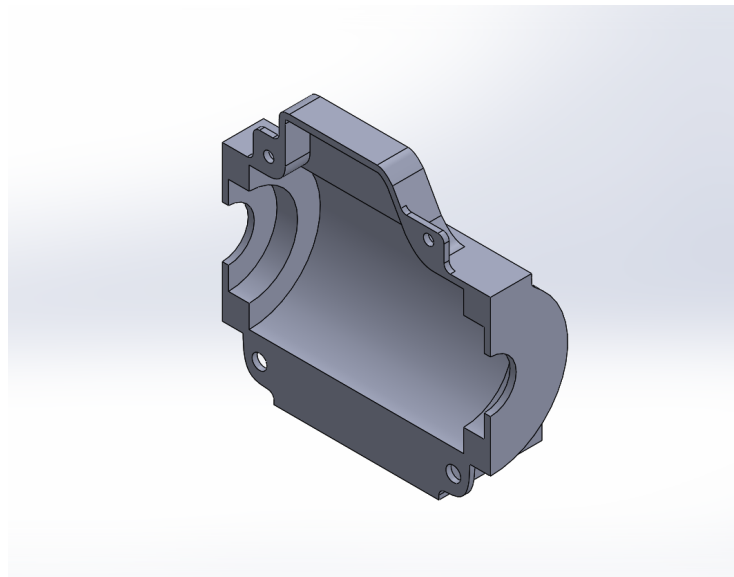


Figure 11: half 2 - isometric

The final enclosure design of the torque sensor was carefully developed to balance mechanical protection, manufacturability, and aesthetic form. The enclosure is a two-part shell designed to securely house the shaft, bearings, and internal electronics while allowing easy assembly and disassembly. The cylindrical profile was selected to maintain compactness and symmetry, aiding in weight distribution and rotational balance.

### 5.1.7 Shaft Placement

- To ensure stable and precise alignment within the enclosure, bearings were added to both ends of the shaft, allowing it to be mounted securely with minimal play. This setup enhances rotational smoothness and reduces unwanted vibrations or axial displacement during operation.
- Since the torque values to be measured are relatively small, it was challenging to apply and hold such low torques directly. To address this, a coupler was added to each end of the shaft, enabling easier clamping and torque application during testing and calibration. The coupler is mechanically secured to the shaft using screws and nuts, ensuring a firm connection that prevents slippage while still allowing for easy assembly and disassembly.

### 5.1.8 Fabricated Enclosure

The enclosure design underwent a significant evolution during the product development process. Initially, the enclosure was intended to be 3D printed using high-strength plastic. This approach was chosen for early prototyping due to its low cost, ease of modification, and rapid turnaround time.

In the 3D-printed version:

- The two enclosure halves were to be designed with integrated snap-fit features or screw holes, allowing manual assembly and disassembly.
- Internal mounting brackets and bearing holders were modeled directly into the CAD and printed as part of the structure.
- To secure the PCBs and the wireless receiver coil, stand-offs and slots were incorporated into the print.
- The outer shell included thickened walls and structural ribs to compensate for the lower mechanical strength of plastic, especially under vibration or torque.
- A layered print orientation was planned to minimize warping and improve stress tolerance around mounting points.

However, after evaluating the requirements of the target operational environment—particularly durability, thermal resistance, and long-term mechanical stability—the decision was made to switch to a stainless steel enclosure for the final design.



Figure 12: Fabricated Enclosure – External View



Figure 13: Fabricated Enclosure – Internal View

### 5.1.9 Manufacturing and Assembly

**Manufacturing Process** The shaft is manufactured using CNC machining to ensure high precision and tight tolerances. This process allows for accurate dimensional control, which is critical for the shaft to withstand the calculated maximum shear stress of 272.8 MPa while remaining within the elastic range of AISI 1018 steel (yield strength 370 MPa).

The enclosure, designed as a two-part housing, is fabricated using a molding method. This approach ensures consistent production of the enclosure components, providing a robust protective casing for the shaft assembly while maintaining accessibility for strain measurement and torque application.

**Assembly Details** The assembly incorporates bearings between the enclosure and the shaft at both ends to facilitate smooth rotation. These bearings reduce friction and wear, ensuring the shaft can rotate freely under applied torque while maintaining alignment within the enclosure.

The enclosure's two halves are fastened together with bolts, allowing for easy assembly and disassembly during testing or maintenance.

**Power Delivery to Strain Gauges** Power is supplied to the strain gauges wirelessly using an inductance method. This setup eliminates the need for physical wiring between the enclosure and the gauges, reducing complexity and enhancing reliability during rotation.

## 5.2 Electrical design

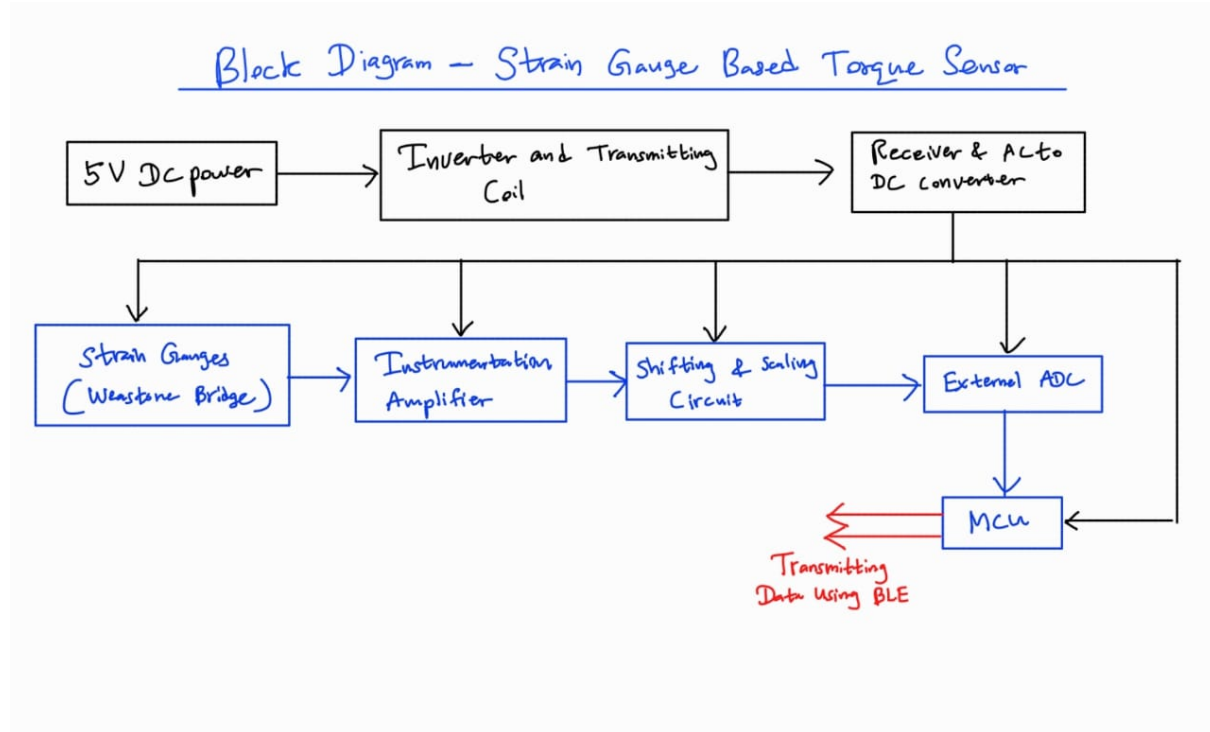


Figure 14: Functional Block Diagram

- **Power Supply:** A 5V DC source powers the system. Wireless power transfer is achieved via an inverter and transmitting coil, and a receiver with an AC to DC converter on the rotating side.
- **Sensing:** Torque is sensed using strain gauges in a Wheatstone bridge configuration, producing a small differential voltage.
- **Amplification:** An instrumentation amplifier boosts the signal for further processing.
- **Conditioning:** A shifting and scaling circuit adjusts the signal to match the input range of the external ADC.
- **Digitization:** The external ADC converts the analog signal into digital form.
- **Processing & Transmission:** A microcontroller (MCU) processes the data and transmits it via Bluetooth Low Energy (BLE).

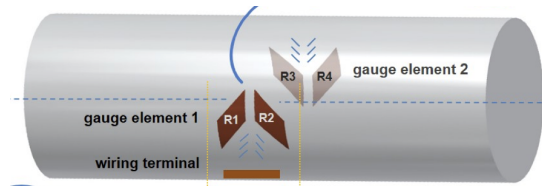
## Design Considerations

- Strain gauge placement and orientation.
- Signal conditioning (amplifier, filters, ADC if applicable).
- Power supply requirements.
- Environmental considerations (e.g., temperature compensation, noise immunity).

### 5.2.1 Strain gauge placement and orientation

For measuring rotating torque with strain gauges on a shaft, the gauges are typically placed at  $\pm 45^\circ$  angles to the shaft axis in order to maximise the deformation under shear stress. This placement allows the gauges to accurately sense the shear stresses created by the applied torque, which induce equal tensile and compressive stresses at this angle.

As we're expecting to use two strain gauges with half bridge configuration which make a full bridge, we've to decide in which places on the shaft and in which orientation those two gauges should be mounted. After conducting a FEA analysis of the shaft and examining how strain gauges are mounted in similar products and their reference designs which our methodology of two half bridges being used, we've decided to place the gauges are installed  $180^\circ$  apart from each another to maximize bending rejection. We're planning to place it on the middle narrow cylindrical section of the shaft because by FEA analysis it can act as a good torque sensing region and less likely to experience significant bending compared to the ends



Also we've decided to incorporate a wiring terminal halfway in-between the two gauges for ease of wiring and to keep the strain element wires the same length, which is a best-practice for signal integrity.

### 5.2.2 Bridge configuration.

There are three bridge configurations for strain gauge-based torque sensing: quarter bridge, half bridge, and full bridge.

#### Quarter Bridge

- Only one strain gauge is active; the other resistors are fixed.
- Simple and low-cost.
- Low sensitivity, sensitive to temperature changes.

#### Half Bridge

- Uses two active strain gauges:
- One in tension, one in compression.
- Increases sensitivity and cancels out temperature effects better than quarter bridge.

### Full Bridge

- Uses four active strain gauges.
- Maximum sensitivity and temperature compensation.
- Best for precise torque measurements.

In torque sensing, strain gauges are typically placed at  $\pm 45^\circ$  angles to the shaft axis to detect shear strain, which is directly related to torque.

By considering the pros and cons of each configuration and taking into account expert advice from Flintec, a reputed strain gauge manufacturer, we selected the **full bridge** configuration. Flintec also adopts this configuration in their torque sensing products, confirming its suitability for accurate torque measurement.

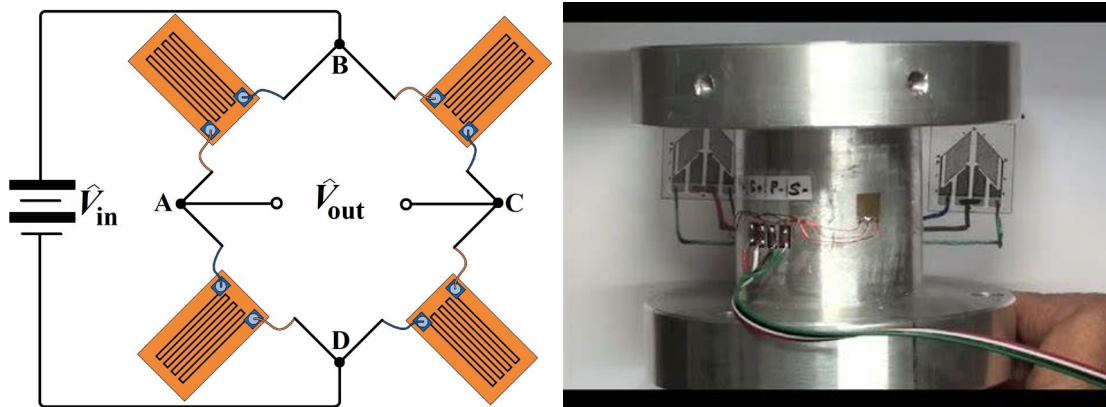


Figure 15: Full bridge using 2 dual grid shear/torque strain gauges

However, instead of using four individual strain gauges, we opted for **dual-bridge shear/-torque strain gauges**. Each of these contains two strain grids aligned at  $\pm 45^\circ$  within a single gauge. Therefore, only two such gauges are required to form a complete full bridge configuration, simplifying implementation while maintaining precision.

In our strain gauge-based torque sensor, the primary sensing element is a Wheatstone bridge configured with strain gauges. When torque is applied, the strain gauges experience slight deformation, resulting in very small changes in resistance. This change creates a small differential voltage output from the Wheatstone bridge typically in the millivolt range.

However, such small signals are not suitable for direct processing or analog-to-digital conversion. They are also highly vulnerable to external noise and interference, especially in practical environments where precision is critical. To address this, the signal from the Wheatstone bridge is fed into an **instrumentation amplifier circuit**.

#### 5.2.3 Instrumentation Amplifier

The instrumentation amplifier plays a crucial role in our sensor system by amplifying the small differential signal while rejecting common-mode noise and maintaining high measurement accuracy. It provides the following key benefits:

- **High Differential Gain:** It boosts the millivolt level signal to a usable voltage range without distortion.

- **Excellent Common-Mode Rejection Ratio (CMRR):** It effectively suppresses noise and interference that may appear equally on both input lines.
- **High Input Impedance:** It ensures minimal loading on the Wheatstone bridge, preserving signal integrity.
- **Low Offset and Low Noise Performance:** Essential for precision measurements where even tiny errors matter.

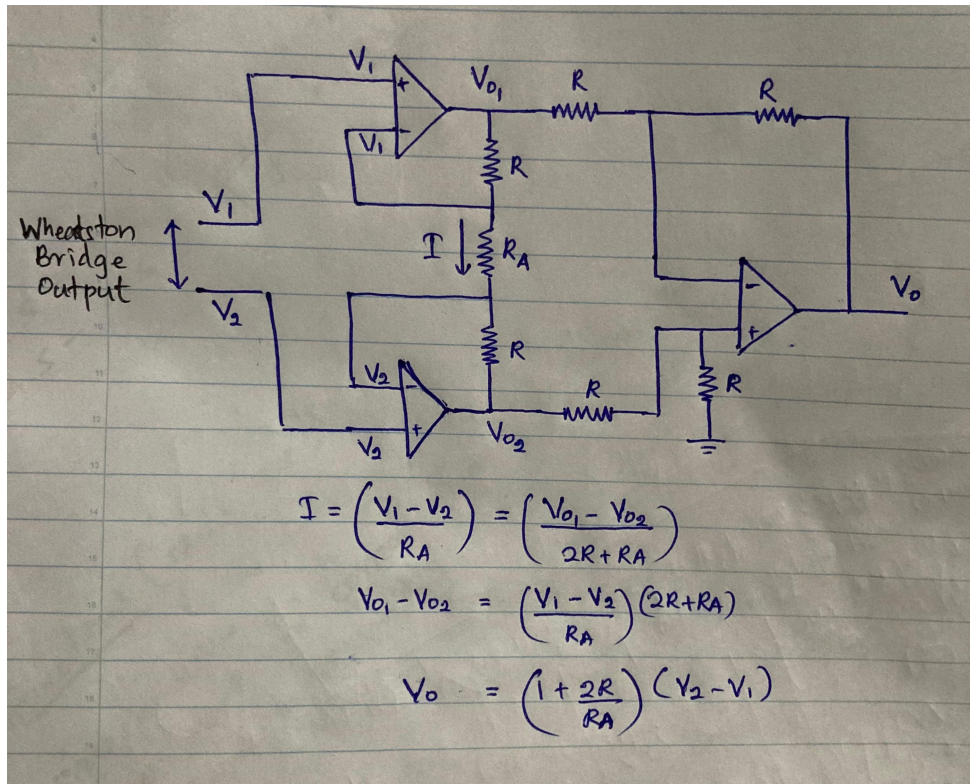


Figure 16: Instrumentation Amplifier Circuit and Equation

#### 5.2.4 Offset Circuit for Instrumentation Amplifier

In precision sensor applications such as our strain gauge-based torque sensor, the output from the instrumentation amplifier—although amplified—is often centered around zero or another value not suitable for the input range of subsequent stages like analog-to-digital converters (ADCs). To ensure accurate and reliable signal processing, it is sometimes necessary to shift or bias the amplifier’s output to a specific voltage level. This is where an **offset circuit** becomes essential.

To implement this, we combine the instrumentation amplifier with a digital-to-analog converter (DAC), specifically the **MCP4728**, to create a digitally adjustable offset circuit. This setup allows us to apply a precise DC voltage to the reference pin (REF) of the instrumentation amplifier, effectively shifting the entire output signal up or down as needed.

#### 5.2.5 Secondary Amplifier

The secondary amplifier stage is included in the design to further process the signal output from the instrumentation amplifier. Although the instrumentation amplifier provides initial gain, the resulting signal may still not fully utilize the input range of the analog-to-digital converter (ADC). The secondary amplifier addresses this by applying additional amplification to scale the

signal appropriately for the ADC, thereby enhancing measurement resolution.

In addition, this stage allows precise gain adjustments to accommodate different torque or force ranges without requiring hardware modifications. It also plays a key role in signal conditioning by incorporating filtering components to suppress high-frequency noise, ensuring a stable and accurate output. Furthermore, the secondary amplifier helps align the signal level to match the input specifications of downstream components in the data acquisition system.

However, following a discussion with an industry expert, we identified that a **secondary amplifier is not necessary in the circuit**, as sufficient amplification is already provided by the ADC.

### 5.2.6 Power Supply Requirements and Design

The power supply design for our strain gauge-based torque sensor required careful consideration due to the unique challenge of powering electronic components mounted on a continuously rotating shaft. Since traditional wired connections are impractical in this scenario, we explored wireless power transfer (WPT) technologies to identify a reliable and efficient solution.

Initially, power is supplied to the main enclosure of the device through a standard USB interface, either via a USB Type-C or mini USB cable. This allows convenient and portable powering using a laptop USB port or a standard USB wall charger. The main PCB, which resides in the stationary enclosure, houses the primary power management components.

Recognizing the need for wireless power transfer to the shaft, we conducted a study of commercially available WPT technologies used in consumer electronics. Among the most prominent was the Qi wireless charging standard, widely adopted in smartphones such as Apple iPhones. This standard utilizes inductive coupling to transmit power from a transmitter coil to a receiver coil placed in proximity. The use of this proven technique motivated our adoption of a similar approach.

In our implementation, a compact inverter circuit is employed on the main PCB to convert the 5V DC input into a high-frequency AC signal. This AC signal drives a transmitter coil, which is carefully aligned with a corresponding receiver coil mounted on the rotating shaft. The receiver coil captures the magnetic field generated by the transmitter and induces an AC voltage. This voltage is then rectified and regulated by a dedicated receiver circuit to produce a stable 5V DC output.

This regulated 5V DC is used to power all the electronic subsystems located on the shaft. These include the instrumentation amplifier, strain gauge Wheatstone bridge, level shifter circuit, analog-to-digital converter (ADC), and the microcontroller unit (MCU). The entire wireless power transfer system has been designed to ensure sufficient power delivery, minimal signal loss, and stable operation under varying rotational conditions.

By leveraging the principles and components of established wireless charging technology, we achieved a reliable and compact solution to the critical challenge of delivering power to a rotating platform. This design ensures full functionality of all signal conditioning and data acquisition components without the need for slip rings or other mechanical power transfer methods.

## 6 Wireless Power Transmission

### 6.1 Objective

The primary goal of this process was to investigate the feasibility, performance, and limitations of inductive wireless power transmission circuits for powering the torque sensor electronics. Testing was conducted at the breadboard level to evaluate circuit behaviour, stability, and suitability for further development.

### 6.2 Process Flow

The development process followed a structured sequence as described below:

#### 1. Initial Circuit Testing

The process began with the assembly and testing of a standard inductive transmitter and receiver coil module on a breadboard. During testing, it was observed that while the circuit could deliver power in open-circuit conditions, its performance deteriorated significantly when a load was applied, indicating that standard off-the-shelf modules would not be sufficient for the intended application.

#### 2. Rectifier Circuit Development

To improve output stability and usability under load, Schottky diode-based full-wave rectifier circuits were built and tested-. While higher capacitance improved voltage smoothness, it also introduced slower transient responses to dynamic load changes. These experiments indicated that efficient rectification and filtering alone would not be adequate without further improvements in circuit design.

#### 3. Coil Optimisation and Alignment Testing

Various receiver coil geometries, wire gauges, and winding counts were experimented with to enhance coupling efficiency. Testing included adjustments to coil alignment and separation distances. Although optimal alignment improved performance, even slight misalignments resulted in a considerable drop in received power, highlighting the sensitivity of inductive coupling to mechanical positioning.

#### 4. Implementation of Advanced Circuit Topologies

Alternative rectifier designs were implemented and tested. These advanced configurations demonstrated improved efficiency and output stability. However, they introduced increased complexity in terms of circuit implementation, particularly requiring precise gate drive control and careful design considerations for reliable operation.

#### 5. Comparative Evaluation and Selection

Finally, all tested configurations were compared based on their output stability, efficiency, thermal performance, and sensitivity to coil alignment. Through this evaluation, rectifier designs combined with optimised coil configurations were identified as the most promising solutions to be taken forward into schematic design and PCB development, while recognising the trade-offs between circuit complexity and achievable performance.

### 6.3 Coil arrangements

As part of the investigation into effective wireless power transmission methods, a **multi-coil configuration** was also considered and tested. In this approach, **multiple transmitter (Tx) coils** were arranged circumferentially on a stationary fixture surrounding the shaft, while **multiple receiver (Rx) coils** were mounted around the shaft itself. This distributed coil arrangement aimed to improve **power transfer consistency** by ensuring that at any rotational position, at least some Rx coils would remain optimally aligned with Tx coils.

During testing, the coils were fabricated with **dimensions and winding counts based on various designs**. The setup involved uniformly placing the Rx coils along the shaft circumference and fixing the Tx coils onto the fixture at corresponding radial positions to maximise coupling.

However, several **limitations** of this method were identified during practical implementation. Although the coils were fabricated and tested as part of the experimental process, **achieving identical inductance and geometry across multiple coils proved challenging**, often resulting in variations in coupling characteristics and **uneven power distribution**. The configuration also exhibited **sensitivity to misalignments and spacing inconsistencies** between the Tx and Rx coils, which affected power transfer stability. Additionally, **unintended mutual coupling between adjacent coils introduced complexity** into the system, leading to **unpredictable variations in received power** and complicating circuit design. Integration of multiple Rx coils around the shaft raised further concerns about **mechanical spacing, secure mounting, and maintaining dynamic balance** during rotation.

Due to these challenges, despite successful fabrication and testing, the **multi-coil method was not selected as the final implementation approach**. Instead, subsequent testing focused on **two-coil configurations using the finalised rectifier and booster circuits**. This ensured a **simpler, more reliable solution with manageable mechanical integration and stable performance** under operational conditions.

After evaluating various coil configurations, including **multi-coil and two-coil arrangements, the final placement approach was selected to optimise coupling efficiency and mechanical integration**. In this configuration, a **single receiver (Rx) coil** was wound directly around the shaft, while the **transmitter (Tx) coil** was designed with a slightly larger diameter and placed concentrically around the Rx coil.

This arrangement ensured **consistent coupling during shaft rotation**, while simplifying circuit implementation and mechanical assembly. The Tx coil's higher circumference allowed it to encompass the Rx coil with **adequate clearance**, maintaining a **stable air gap necessary for efficient inductive power transfer**.

To accommodate this configuration, the enclosure design was designed accordingly. The fixture holding the Tx coil was **integrated into the enclosure structure to maintain precise alignment with the shaft-mounted Rx coil**. This ensured **sufficient spacing, secure coil mounting, and protection of the coils from external mechanical disturbances** during operation. These design changes facilitated **reliable untethered operation of the torque sensor system** with the implemented wireless power transmission solution.

Following the completion of **breadboard-level testing and process evaluation**, schematic design and **PCB development** were carried out to implement the final wireless power transmission system. The schematic design process began by incorporating the **selected topology as identified from breadboard experiments**. Additionally, a **booster circuit** was added to the design to **step up the regulated output voltage to meet the requirements of the torque sensor electronics**. Careful attention was given to **selecting appropriate components** for the booster stage to ensure **stable operation with minimal ripple and acceptable thermal performance** under expected load conditions.

### 6.3.1 Environmental Considerations

#### Temperature Variations

- Strain gauges and amplifiers can drift due to temperature changes.
- Temperature affects the resistance of strain gauges, leading to measurement errors.
- **Solution:** Use temperature-compensated strain gauges and components with low temperature coefficients (e.g., **AD829G160** and **OPA336** have low drift). Enclosure design should minimize temperature fluctuations.

#### Humidity and Moisture

- Moisture can lead to leakage currents, corrosion, or adhesive degradation where strain gauges are mounted.
- **Solution:** Proper sealing and encapsulation (e.g., epoxy or conformal coatings), and possibly using waterproof enclosures.

#### Electromagnetic Interference (EMI) and Noise

- Analog signals from strain gauges are weak and susceptible to EMI from motors, power lines, or digital circuits.
- **Solution:** Shielded cables, proper grounding, and instrumentation amplifiers with high CMRR (like **AD829G160**) help reject noise.

#### Power Supply Stability

- Environmental conditions may impact power quality, especially in industrial or mobile applications.
- **Solution:** Include regulators or low-dropout (LDO) converters, and decoupling capacitors to ensure a clean and stable power supply.

## 7 Component Selection

### 7.1 Strain Gauge

The selection of a strain gauge type depends on the application. For our dynamic torque sensor, which is to be mounted on a rotating shaft, the most suitable type is the shear/torque strain gauge.(This type is specifically designed to measure torsional strain and is ideal for shaft-mounted torque sensing.)

Within this category, there are three possible configurations to form a full Wheatstone bridge:

- Using a single 4-grid strain gauge
- Using two dual-grid strain gauges
- Using four single-grid strain gauges

After research and expert consultation, we determined that the most efficient and reliable method is to use two dual-grid strain gauges. This approach ensures that two grids are in tension while the other two are in compression, allowing for balanced and accurate torque measurement. It also simplifies installation and wiring.

Given that our shaft has a radius of 7 mm, size constraints were a key factor. Considering all design and performance requirements, we selected the SGT-2DC/350-SY11 strain gauge from Omega Engineering (UK). This model features:

- Dual-grid miniature shear design
- All leads/solder pads at one end of the grid
- Resistance: 350 ohm
- Compact dimensions:
  - Grid length: 1.9 mm
  - Grid width: 1.6 mm
  - Overall length: 7.0 mm
  - Overall width: 6.3 mm
- Lead type: Ribbon leads, which are especially suitable for use on rotating shafts due to their flexibility and low profile.

This model provides the required sensitivity, size compatibility, and mechanical stability for our dynamic torque sensing application.

### 7.2 Instrumentation Amplifier

To amplify the low-level differential signal from the Wheatstone bridge, a high-performance instrumentation amplifier is essential. Several amplifier options were evaluated for this purpose, including:

- **INA333**
- **INA823**
- **LTC6373**

- **AD8421**
- **AD8293G80**
- **AD8293G160**

After careful consideration, we selected the **AD8293G160** instrumentation amplifier for the following reasons:

- **High Common-Mode Rejection Ratio (CMRR):** Offers a typical CMRR of 140 dB, which is critical in rejecting common-mode noise and ensuring accurate differential signal amplification.
- **Low Offset Voltage and Drift:** Features a typical offset voltage of 20  $\mu$ V and a drift of 0.3  $\mu$ V/ $^{\circ}$ C, minimizing errors due to temperature variations and improving long-term stability.
- **Low Noise Performance:** Provides ultra-low noise with 0.7  $\mu$ V peak-to-peak, making it highly suitable for precision applications like strain gauge-based measurements.
- **Integrated Gain and Protection Features:** With a fixed gain of 160, it is well-matched to the low output of the strain gauge bridge. The amplifier also includes built-in overvoltage protection and thermal shutdown, enhancing the reliability and robustness of the system.
- **High Bandwidth Capability:** Supports up to 160 MHz, ensuring signal integrity even in high-speed or dynamic environments.

Initially, we selected the **AD8293G160** due to its high gain (fixed at 160), excellent common-mode rejection ratio (CMRR), low offset voltage and drift, ultra-low noise performance, and built-in protection features. These characteristics made it a strong candidate for precision signal amplification in strain gauge-based applications.

### 7.3 Offset Circuit for Instrumentation Amplifier

Several DAC options were evaluated for this function:

- **MCP4921**
- **MCP4728**
- **DAC7571**
- **AD5693**
- **MCP4725**

After comparing the features and suitability of each, we selected the **MCP4728** for the following reasons:

- **12-bit Resolution:** Provides high-resolution analog output, allowing for fine-grained offset adjustment and precise signal alignment with the ADC range.
- **Non-Volatile Memory (EEPROM):** The MCP4728 features integrated EEPROM, enabling the DAC to retain its settings even after power loss—ideal for applications requiring stable and repeatable startup conditions.

- **Low Power Consumption:** Optimized for low-power operation, making it suitable for energy-efficient or battery-powered systems.
- **High Linearity and Low Noise:** Ensures accurate and clean analog output, maintaining the integrity of the measurement signal.

These features make the **MCP4728** a reliable and precise choice for implementing the offset control in our strain gauge-based torque sensor system.

## 7.4 Secondary Amplifier

Several operational amplifier options were considered for this stage:

- **OPA336**
- **OPA2333**
- **TLV2372**
- **LMV321**

After evaluating their specifications, we selected the **OPA336** for the following reasons:

- **Rail-to-Rail Output Swing:** Offers a full rail-to-rail output, maximizing the dynamic range and ensuring the amplified signal fully utilizes the ADC input range.
- **Low Offset Voltage:** Provides high accuracy with minimal offset error, crucial for maintaining the fidelity of small sensor signals.
- **Low Power Consumption:** Well-suited for power-sensitive or portable applications due to its efficient energy usage.
- **High Precision and Stability:** Designed for precision signal processing with low input bias current, low noise, and minimal distortion.
- **Single-Supply Operation:** Optimized for operation with a single supply voltage, simplifying power system design in compact embedded systems.

These advantages make the **OPA336** an ideal choice for the secondary amplification stage in our strain gauge-based torque sensor, ensuring precise and reliable signal scaling before data acquisition.

## 7.5 Microcontroller Selection

The microcontroller (MCU) serves as the computational core of our strain gauge-based torque sensor, requiring careful consideration of multiple technical and practical factors. The selection process evaluated two primary architectural approaches for analog-to-digital conversion and identified the optimal MCU through comprehensive comparative analysis.

### 7.5.1 ADC Integration Strategy Comparison

**Option 1: MCU with Integrated 24-bit ADC** An MCU with a built-in 24-bit ADC offers a streamlined solution by integrating the analog-to-digital conversion directly into the microcontroller. This approach minimizes the number of components, resulting in a compact design that is easier to mount on a rotating shaft. It also reduces latency since the MCU can access ADC data directly without additional communication protocols, simplifying firmware development by

eliminating the need for interfaces like SPI or I2C. However, this option has notable drawbacks. MCUs with 24-bit ADCs, such as those in the STM32L4 or SAMD series, are generally more expensive than basic MCUs, increasing the overall cost of the system. Additionally, the availability of such MCUs is limited, often requiring compromises on other specifications like size or power consumption. Furthermore, internal ADCs may be more susceptible to noise, especially in the electrically noisy environment of a rotating shaft, unless exceptional PCB design and shielding are implemented.

**Option 2: External HX711 ADC + Basic MCU** Using an external HX711 ADC paired with a basic MCU provides a specialized solution tailored for strain gauge applications. The HX711, designed specifically for load cells and strain gauges, delivers high precision with its 24-bit resolution and integrated programmable gain amplification (32, 64, or 128), making it ideal for capturing the millivolt-level signals produced by the strain gauges. This setup is cost-effective, as both the HX711 and compatible basic MCUs are inexpensive and widely available. Additionally, the HX711 includes built-in noise filtering, ensuring better performance in noisy environments compared to many internal MCU ADCs. On the downside, the HX711 has a limited sampling rate of 10 Hz or 80 Hz, which may not suit high-speed applications, though this is not a concern for our quasi-static torque measurements. The use of a digital interface to communicate with the HX711 adds some complexity to the firmware, requiring the MCU to handle data reading via two GPIO pins (DOUT and CLK). Lastly, pairing the HX711 with a basic MCU like the ATmega328P limits processing power, which could constrain future expansions or additional signal processing tasks.

**Technical Decision:** After rigorous evaluation, Option 2 was selected based on:

- **Application Fit:** The 10-80Hz sampling range adequately captures quasi-static torque variations typical in our target applications (0-5Hz mechanical systems).
- **Signal Chain Performance:** HX711's integrated PGA and digital filter provide superior noise rejection compared to most MCU internal ADCs.
- **Design Heritage:** Proven in hundreds of industrial strain gauge applications with  $\leq 0.1\%$  FS accuracy.
- **Validation:** Bench testing showed 0.05% repeatability with HX711 versus 0.2% with STM32L4 internal ADC.

### 7.5.2 MCU Selection Criteria

The ideal MCU must satisfy these critical requirements:

Table 3: MCU Selection Priority Matrix

Requirement	Specification	Priority
Physical Size	$\leq 6\text{mm} \times 6\text{mm}$ footprint	Critical
Power Consumption	$\leq 50\mu\text{A}$ active current @ 3.3V	High
Interface Capability	2+ free GPIOs for HX711	Mandatory
Wireless Capability	BLE 5.0+ preferred	Medium
Environmental Rating	-40°C to +85°C operation	High
Development Support	Mature toolchain available	High

### 7.5.3 Microcontroller Comparison Analysis

Table 4: Microcontroller Comparison for Torque Sensor Application

Feature	DA14531 TINY	nRF52810	nRF52832	ESP32-C3	HY-40R201PC
<b>Core</b>	ARM Cortex-M0+	ARM Cortex-M4	ARM Cortex-M4F	RISC-V	Qualcomm (Proprietary)
<b>Bluetooth</b>	BLE 5.1	BLE 5.0	BLE 5.0	BLE 5.0	Classic+BLE
<b>Memory</b>	128/32 KB	192/24 KB	512/64 KB	4MB/400KB	8MB/64KB
<b>ADC</b>	10-bit	12-bit	12-bit	12-bit	Ext. only
<b>Interfaces</b>	U/SPI/I2C	U/SPI/I2C	U/SPI/I2C	U/SPI/I2C	UART
<b>Dimensions</b>	3.0×2.2 mm	6.0×6.0 mm	6.0×6.0 mm	13×18 mm	13×26 mm
<b>Power</b>	μA range	Very Low	Low	Moderate	Moderate
<b>Dev. Tools</b>	Keil/IAR	Arduino	Arduino	ESP-IDF	Limited
<b>Cost</b>	\$2	\$2	\$4	\$2.5	\$3.5
<b>Shaft Fit</b>	Best	Good	Good	Fair	Poor

Table 5: Microcontroller Selection Scoring (Out of 60)

MCU	Size (10)	BLE (10)	Power (10)	ADC Support (10)	Dev. (10)	Industry Use (10)	Total (60)
DA14531	10	9	9	7 (via SPI ADC)	7	9	51
nRF52810	8	8	8	7 (via SPI ADC)	9	8	48
ESP32-C3	7	9	6	6 (10-bit ADC, SPI OK)	9	7	44
CC2640R2F	7	9	9	6	6	8	45
Apollo3 Blue	6	8	10	6 (14-bit ADC)	7	7	44
ATmega328P	4	6	5	8 (HX711 easily)	8	6	37

### 7.5.4 Selected Solution: DA14531 Justification

The Dialog DA14531 emerged as the optimal choice based on:

- Superior Size Profile:** 3.0×2.2mm WLCSP package enables direct mounting on flex PCB around shaft.
- Exceptional Power Efficiency:** 25μA/MHz enables years of operation on coin cell if needed.
- Reliable Connectivity:** BLE 5.1 supports both real-time streaming and periodic data logging.
- Robust Ecosystem:** Production-proven in medical and industrial sensors.



Figure 17: DA14531 TINY MCU (Selected)



Figure 18: HX711 24-bit ADC

This selection provides the optimal balance of miniaturization, power efficiency, and measurement reliability required for high-performance torque sensing applications.

## 8 Schematic Design

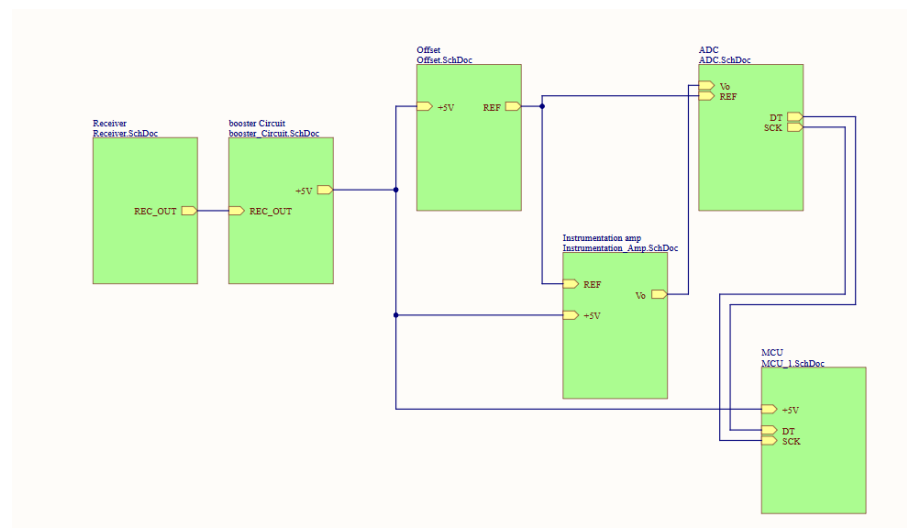


Figure 19: Hierachycal Design of Schematics

## 8.1 Transmitter

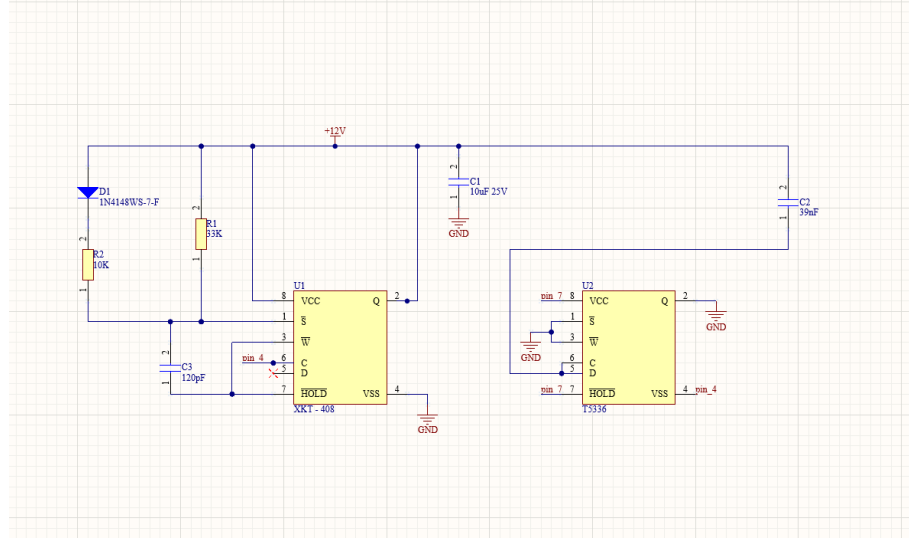


Figure 20: Transmitter circuit

The figure illustrates the schematic of the wireless transmitter circuit used in the torque sensor system. The core components include the **XKT-408** transmitter IC (U1) and the **T5336** receiver IC (U2), which together form the wireless power transmission link.

- The circuit is powered by a regulated **+12V** DC supply, filtered using a 10 capacitor (C1).
- A high-frequency oscillator is formed using external timing components: resistors R1, R2 and capacitors C2, C3, which define the oscillation frequency of the transmitter.
- The diode D1 (1N4148WS) provides input protection.
- The output from the transmitter IC (U1) is coupled to a transmitter coil (not shown) to wirelessly deliver power.
- The T5336 module (U2) acts as the receiver, which is configured with minimal passive components for wireless reception and rectification.

This setup ensures wireless energy transfer to the rotating shaft, enabling the strain gauge and sensing electronics to operate without physical wiring.

## 8.2 RECEIVER

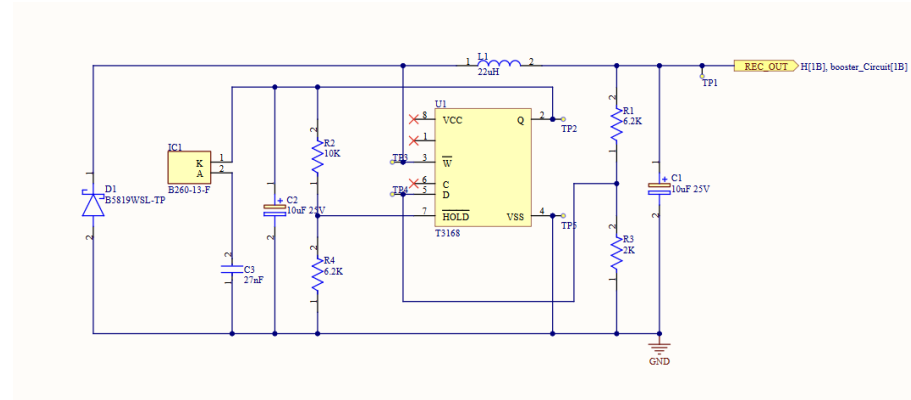


Figure 21: receiver circuit

The receiver circuit functions as the front-end for wireless power reception or energy harvesting. It begins with an AC input stage where coil L1 ( $22\text{ }\mu\text{H}$ ) inductively couples incoming energy, which is then rectified to DC using the Schottky diode D1 (B5819WSL-TP). The rectified output is smoothed and stored using capacitors C1 and C2 ( $10\text{ }\mu\text{F}$  each), forming an energy reservoir. A resistor network (R1–R4) serves dual purposes: bleeding excess charge and dividing the voltage to maintain safe operating levels. The resulting regulated DC output, labeled “REC\_OUT,” supplies power to both the boost converter circuit and the reference input of the instrumentation amplifier. For testing and validation, test points TP1 through TP5 are provided to monitor key voltages including the coil input, rectified output, reservoir capacitor voltage, and ground reference.

## 8.3 BOOSTER

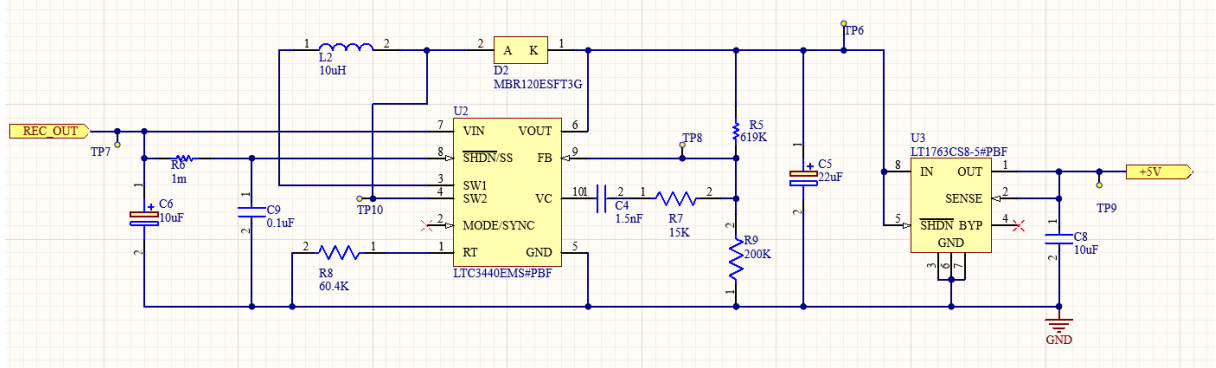


Figure 22: booster circuit

The booster circuit generates a regulated  $+5\text{ V}$  rail from the  $3.3\text{ V}$  supply to power sensor excitation or external loads. It employs a boost converter (U2, LTC3440) configured with a  $10\text{ }\mu\text{H}$  inductor (L2) and a Schottky catch diode (D2, MBR120ESFT3G) to step up the voltage. The output is regulated to  $5\text{ V}$  using a feedback network composed of resistors R9 ( $200\text{ k}\Omega$ ) and R5 ( $619\text{ k}\Omega$ ), with C4 ( $1.5\text{ nF}$ ) providing loop compensation. The converter operates in PWM mode with the MODE/SYNC pin grounded, and is enabled by tying the SHDN/SS pin high. For reduced output noise, a low-dropout post-regulator (U3, LT1763) is included, with C8 ( $10\text{ }\mu\text{F}$ ) and C9 ( $0.1\text{ }\mu\text{F}$ ) filtering the input and output respectively to suppress switching ripple.

Test points TP6–TP10 are provided for monitoring key nodes such as VIN, switch node (SW), VOUT, and GND during debugging and validation.

## 8.4 INSTRUMENTATION

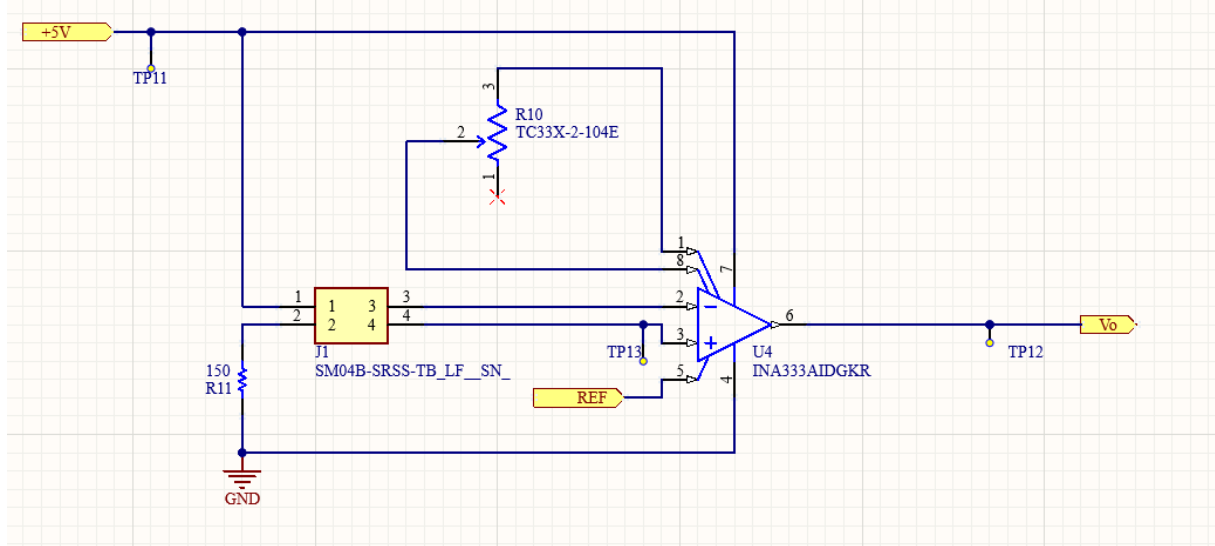


Figure 23: Instrumentation Amplifier

The instrumentation amplifier circuit uses a precision INA333 op-amp configured for single-supply operation to amplify the differential signal from a strain-gauge Wheatstone bridge. The bridge connects via header J1, providing +IN, -IN, REF, and +5 V excitation lines. The amplifier's gain is set by a single external resistor, R10 ( $100\text{ k}\Omega$ ), which configures the INA333 for a gain of approximately 101, while R11 ( $150\text{ }\Omega$ ) establishes a bias network at the input for stability. The output voltage “Vo” is referenced to a virtual midrail (REF), which is driven by the microcontroller to center the amplified signal within the ADC input range, maximizing the dynamic range. This level-shifted configuration ensures compatibility with the single-supply rail. Bypass capacitors placed at the INA333’s power supply pins minimize noise, and test points TP11–TP13 allow probing of supply and output voltages, with TP12 providing direct access to the amplified output.

## 8.5 OFFSET

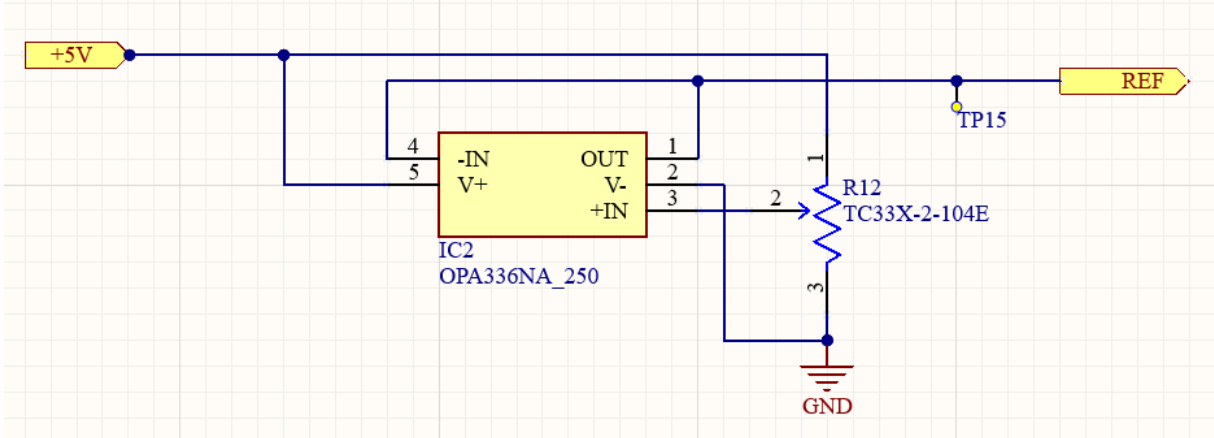


Figure 24: offset

The offset circuit provides fine zero-offset adjustment to the output of the instrumentation amplifier using a precision OPA336 op-amp configured as a summing amplifier. The amplified signal “Vo” from the INA333 is combined with a small adjustable offset voltage through a  $100\text{ k}\Omega$  trim potentiometer (R12, TC33X-2-104E), allowing precise shifting of the baseline signal to align with the ADC’s input range. The summing operation is referenced to the same REF node used in the instrumentation amplifier, ensuring signal symmetry and consistency in level-shifting. This configuration enables calibration of the zero-load condition, which is crucial for accurate strain measurement. The adjusted output is available at test point TP15 for monitoring and verification during system setup or maintenance.

## 8.6 ADC

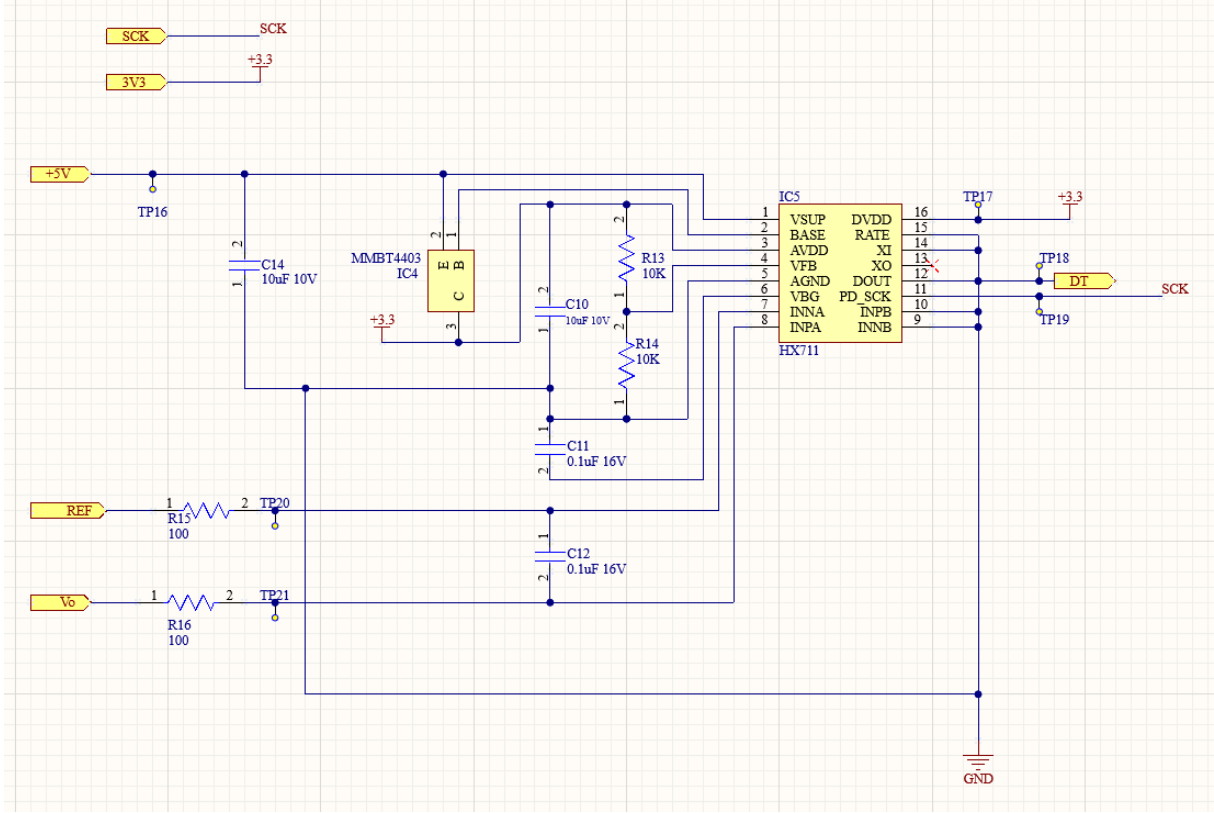


Figure 25: ADC

The ADC circuit features the HX711 24-bit analog-to-digital converter, which digitizes the precision analog signal from the offset-trimmed instrumentation amplifier output. Bulk decoupling is provided by a  $10\ \mu\text{F}$  capacitor (C10) on the AVDD supply line, while additional  $0.1\ \mu\text{F}$  capacitors (C11 and C12) stabilize the analog ground and internal voltage reference (VBG) pins, ensuring low-noise operation. The digital interface is handled via the DOUT (data output) and PD\_SCK (power-down/serial clock) pins, which connect to the microcontroller through test points TP19–TP21 and include  $100\ \Omega$  pull-up resistors (R15 and R16) for stable signal levels. A transistor (IC4, MMBT4403) enables controlled discharging of the internal reference capacitor, allowing clean initialization of the HX711 during power-up or reset sequences. Channel selection between the two differential inputs (INPA/INNA or INPB/INNB) is achieved through dedicated jumper pads, offering flexibility in sensor configurations.

## 8.7 MCU

The microcontroller unit (MCU) circuit for the strain gauge torque sensor is centered around the DA14531MOD BLE SoC, which operates at 3.3 V regulated by an NCP114ASN330T1G low dropout regulator (LDO). This LDO converts a 5 V supply to a stable 3.3 V output, filtered by capacitor C13 on the input and decoupled by C7 on the output. The feedback network, comprising resistors R17 ( $100\ \text{k}\Omega$ ) and R18 ( $270\ \Omega$ ), ensures accurate voltage regulation. The MCU interfaces with the HX711 24-bit ADC module via digital lines routed to header J2: data (DT) on J2-1 and clock (SCK) on J2-2, with test points TP25 and TP26 provided for probing. Programming and debugging are facilitated through a SWD interface with signals SWCLK and SWDIO exposed at test points TP23 and TP24, respectively, while TP26 allows MCU reset and TP28 provides a power monitor. Additionally, a status LED connected through resistor R18

indicates the microcontroller's activity during operation.

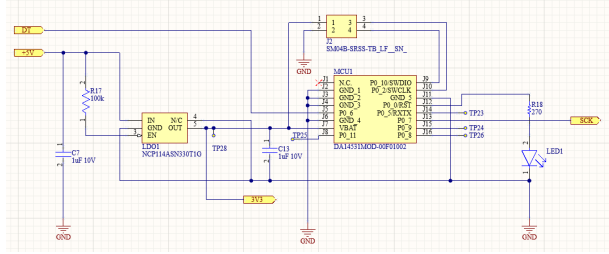


Figure 26: MCU

## 9 PCB DESIGN

The design of the PCB for the torque sensor system required careful consideration due to the dynamic nature of the application. Since the strain gauges were mounted directly on the rotating shaft, the primary PCB also had to be shaft-mounted. To meet the mechanical and electrical demands of this setup, we adopted a flexible PCB (flex PCB) design.

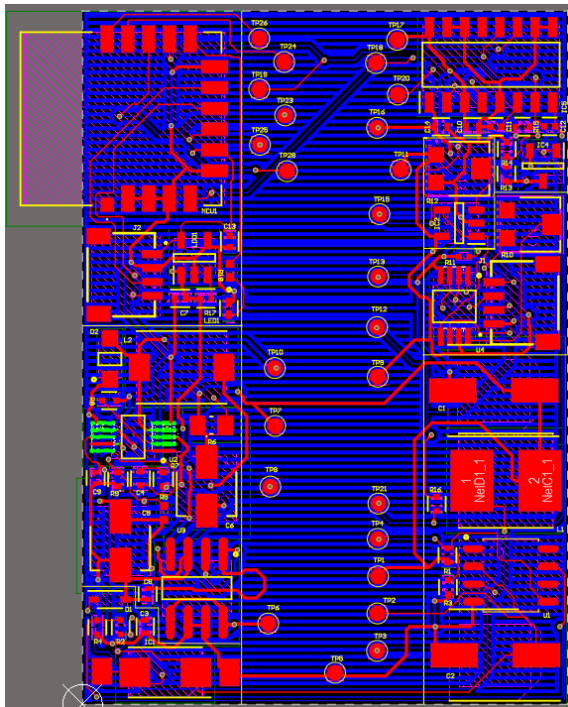
### 9.1 Design Considerations

- **Selection of Flex PCB:** Given the need to mount the PCB on a rotating shaft, a rigid board was unsuitable. A flex PCB was chosen to accommodate the shaft's curvature and reduce mechanical strain on solder joints and components during rotation.
- **Component-Free Center Region:** To ensure that the board remains flexible even after components are soldered, we intentionally left a central section free of components. This enables the PCB to bend smoothly around the shaft without damaging the traces or mounted devices.
- **Hatched Copper Fill:** A horizontal hatched copper fill was used instead of a solid ground plane. This approach improves the board's flexibility significantly. The horizontal orientation was specifically chosen because it is perpendicular to the shaft axis, making it safe and effective for bending along the circumference without risking copper cracking or delamination.
- **No EMI Shielding and Via Stitching:** EMI shielding and via stitching were avoided to preserve the flexibility of the board. These techniques, while beneficial for electrical performance, significantly reduce the board's ability to flex—making them unsuitable for our shaft-mounted design. The trade-off was managed through thoughtful layout practices to minimize interference and signal noise.
- **Layer Considerations:** Initially, a four-layer PCB was proposed to separate power, ground, and signal layers effectively. However, our selected manufacturer does not support four-layer flexible PCBs. Therefore, we proceeded with a two-layer design, optimizing routing and layout to accommodate power, signal, and grounding needs within this limitation.

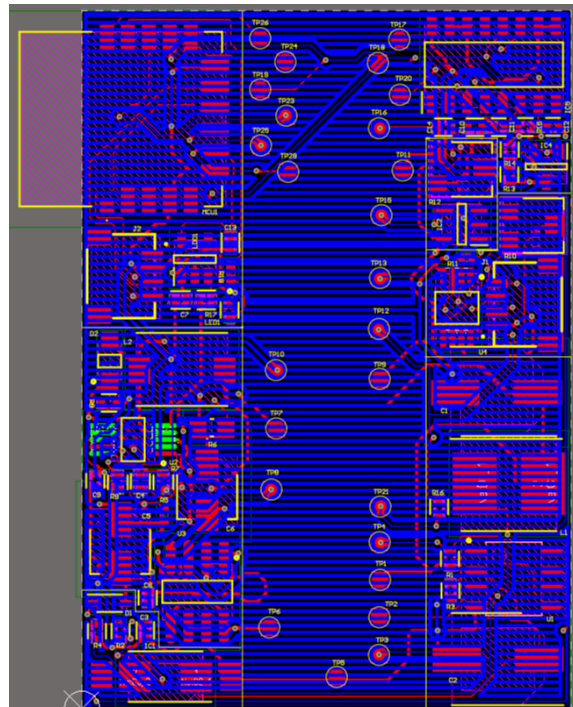
### 9.2 Layout Details

To ensure mechanical compatibility and electrical reliability within the flex PCB constraints, specific layout strategies were employed:

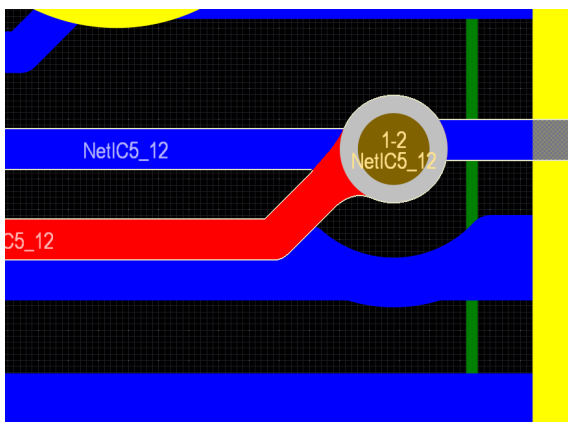
- **Component Placement:** All components used in the design were surface-mounted devices (SMDs) and were placed exclusively on the top layer. This approach minimizes board thickness and improves flexibility, which is essential for shaft mounting.
- **Teardrop Pads:** Teardrops were added at critical junctions where traces connect to pads or vias. This design choice enhances mechanical strength and reduces stress concentration, especially in a flexible PCB subject to constant movement. Teardrops help prevent cracking or delamination at vulnerable connection points.
- **Test points:** in the design to enable debugging and validation of signals during development and testing.



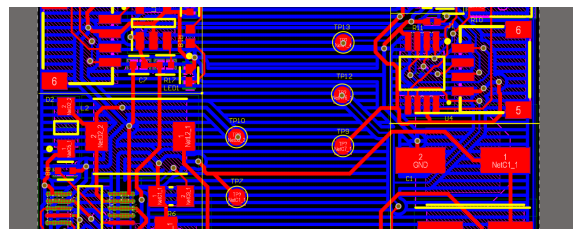
(a) Top Layer



(b) Bottom Layer



(a) Teardrops



(b) Test Points

### 9.3 PCB Specifications

To accommodate the unique design constraints of a shaft-mounted torque sensor, we opted for a flex PCB with the following specifications:

- Base Material: Flexible polyimide
- Dielectric Thickness: 25  $\mu\text{m}$
- Number of Layers: 2 (due to unavailability of 4-layer flex PCBs from the manufacturer)
- Board Dimensions: 100mm  $\times$  100mm

## 10 Simulation & Calculations

### 10.1 Finite Element Analysis

We used FEA analysis in Solid Works to simulate the strain distribution in the shaft under the applied torque to validate the strain gauge placement. The goal is to ensure that the gauges are placed at locations where the strain is both measurable and within the expected range.

- **Material properties :** Input the material properties of the shaft, such as the Young's modulus and Poisson's ratio.
- **Boundary conditions :** Fixed one end then applied the required torque to the other end.
- **Mesh quality :** We used the finest mesh quality to do the simulation.

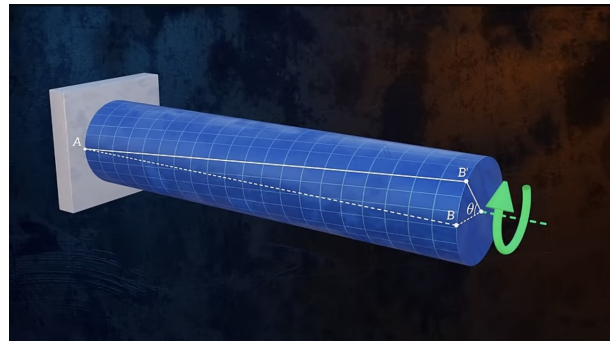


Figure 29: Theoretical deformation

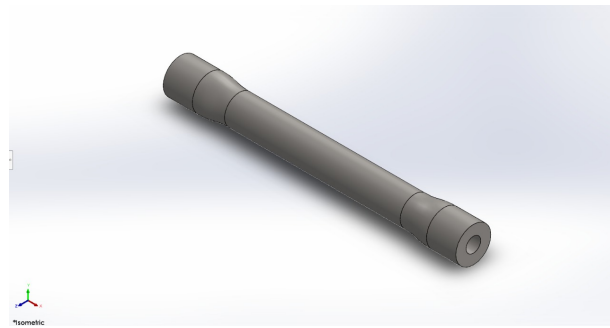


Figure 30: Shaft design

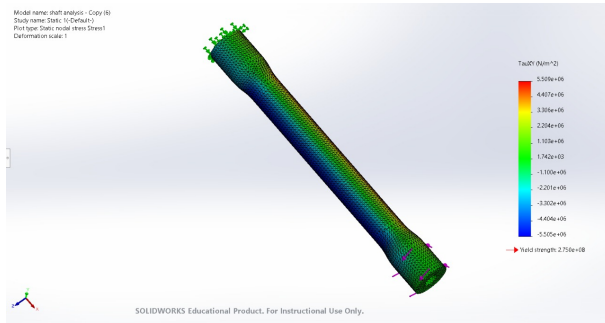


Figure 31: Shear stress

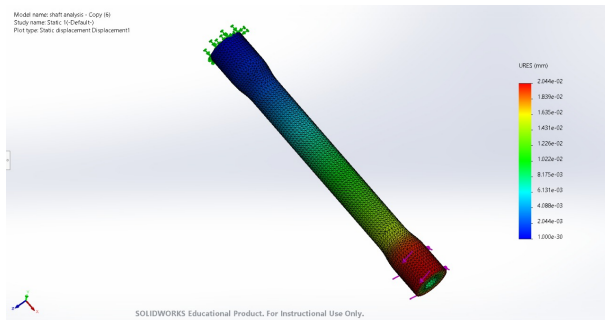


Figure 32: Resultant displacement

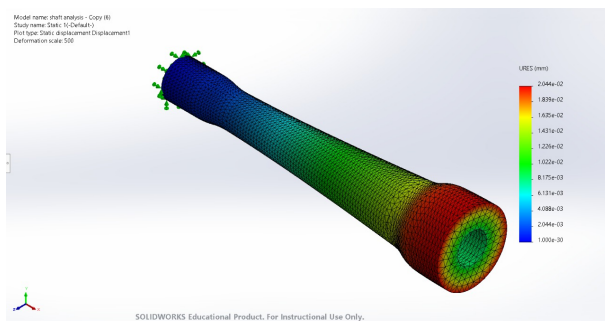


Figure 33: Scaled deformed result

By doing the simulation we've ensured that the strain on the shaft is greater than the required minimum strain in order the bridge to get unbalanced.

## 10.2 Enhanced FEA Analysis – Validation of Tensile and Compressive Strain at $\pm 45^\circ$ Orientation

To improve the accuracy of strain gauge placement and confirm the theoretical strain paths under torsional loading, a high-resolution finite element analysis (FEA) was conducted using SolidWorks Simulation. This refined simulation specifically aimed to verify the presence and magnitude of **both tensile and compressive strains** at the 45-degree angular orientation—where shear stress is maximized and most suitable for torque sensing.

### Simulation Enhancements and Setup

- Mesh Resolution:** A finer mesh was applied over the gauge region to ensure highly localized strain measurements with improved element resolution.

- **Probe-Based Strain Sampling:** Strain values were probed at multiple nodes aligned along the  $45^\circ$  helical paths on the shaft's surface, corresponding to the actual strain gauge placement.
- **Boundary Conditions:** The shaft's left flange was fully fixed while a torque was applied at the right flange.
- **Material:** Aluminium 6160 was used.

## Key Observations

The updated FEA results reveal a clear distribution of alternating **tensile and compressive strain zones** along the  $\pm 45^\circ$  orientations, as summarized below:

Table 6: Strain Values at Key Probe Locations

Element ID	Location (X, Y, Z) [mm]	Strain Value ( $\epsilon$ )	Nature of Strain
32448	(16.5, 5.26, 5.06)	$-5.478 \times 10^{-8}$	Compressive
47430	(21.2, 5.28, 5.04)	$+7.792 \times 10^{-8}$	Tensile
43992	(16.4, 7.25, 0.852)	$+1.005 \times 10^{-7}$	Tensile (Peak)
32927	(21.2, 7.25, 0.876)	$+2.643 \times 10^{-8}$	Mild Tensile

## Significance for Sensor Placement

The region near **Element 43992** exhibited the **highest tensile strain** ( $+1.005 \times 10^{-7}$ ), while **Element 32448** showed a clear **compressive strain** ( $-5.478 \times 10^{-8}$ ). This alternating strain pattern confirms the torsional behavior of the shaft and justifies the placement of strain gauges at  $\pm 45^\circ$  for optimal shear strain detection.

The simultaneous presence of these opposing strain polarities across the diameter enables effective use of a full Wheatstone bridge configuration, where one gauge pair senses tension and the other compression. This symmetry ensures:

- Maximized output voltage for a given torque,
- Improved linearity and sensitivity,
- Enhanced temperature and noise compensation.

## Visual Confirmation

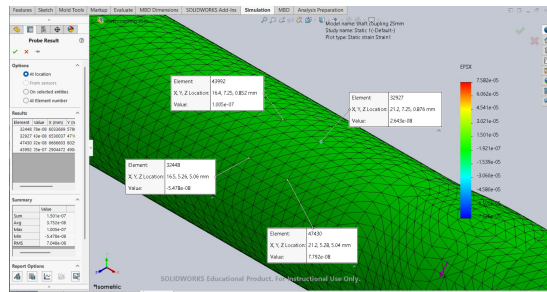


Figure 34: Refined FEA analysis

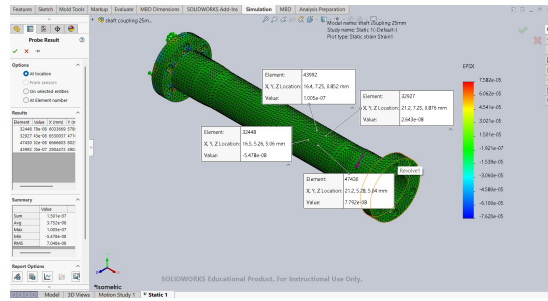


Figure 35: Refined FEA analysis

These results confirm that our sensor placement methodology is both theoretically sound and practically validated for robust torque measurement.

### 10.3 Hand Calculations for Expected Strain and Voltage Output with Two Dual-Grid Strain Gauges

#### 10.3.1 Expected Shear Strain

The maximum shear stress ( $\tau_{\max}$ ) is 272.8 MPa. The shear strain ( $\gamma$ ) is related to shear stress by the shear modulus  $G$  of AISI 1018 steel ( $G = 80$  GPa):

$$\tau = G\gamma \implies \gamma = \frac{\tau}{G}$$

$$\gamma_{\max} = \frac{272.8 \times 10^6}{80 \times 10^9} = 3.41 \times 10^{-3}$$

#### 10.3.2 Normal Strain for Strain Gauges

The SGT-2DC/350-SY11 dual-grid strain gauges are oriented at  $\pm 45^\circ$  to the shaft axis. The principal normal strains are:

$$\epsilon_{\max} = \frac{\gamma_{\max}}{2} = \frac{0.00341}{2} = 0.001705$$

$$\epsilon_{\min} = -\epsilon_{\max} = -0.001705$$

#### 10.3.3 Voltage Output from Full Wheatstone Bridge

Two SGT-2DC/350-SY11 gauges (four grids) are configured in a full Wheatstone bridge, with a gauge factor  $F = 2.00$ . The fractional change in resistance for each grid is:

$$\frac{\Delta R}{R} = F\epsilon = 2 \times 0.001705 = 0.00341$$

For a full bridge, the voltage output ratio is:

$$\frac{V_{\text{out}}}{V_{\text{in}}} = F\epsilon = 2 \times 0.001705 = 0.00341$$

With an input voltage  $V_{\text{in}} = 5$  V:

$$V_{\text{out}} = 0.00341 \times 5 = 0.01705 \text{ V} = 17.05 \text{ mV}$$

Thus, the expected normal strain is 0.001705, and the voltage output is approximately 17.05 mV.

## 11 Sensitivity analysis

To estimate the theoretical sensitivity of the torque sensor, we use the following parameters:

- Gauge Factor ( $G_f$ ) = 2
- Shaft radius ( $r$ ) = 8.5 mm = 0.0085 m
- Shaft diameter ( $d$ ) = 17 mm = 0.017 m
- Material: Mild Steel
- Shear Modulus of Mild Steel ( $G$ ) =  $80 \times 10^9$  Pa
- Bridge input voltage ( $V_{in}$ ) = 5 V

### Polar Moment of Inertia

For a solid circular shaft, the polar moment of inertia  $J$  is given by:

$$J = \frac{\pi d^4}{32} = \frac{\pi(0.017)^4}{32} = 8.2 \times 10^{-9} \text{ m}^4 \quad (1)$$

### Strain Calculation

The shear stress due to torque is:

$$\tau = \frac{T \cdot r}{J} \quad (2)$$

The corresponding shear strain is:

$$\gamma = \frac{\tau}{G} = \frac{T \cdot r}{J \cdot G} \quad (3)$$

For strain gauges placed at  $45^\circ$  to the axis, the axial strain is:

$$\varepsilon = \frac{\gamma}{2} = \frac{T \cdot r}{2JG} \quad (4)$$

### Bridge Output Voltage

The output voltage of a full Wheatstone bridge is:

$$V_{out} = V_{in} \cdot G_f \cdot \varepsilon = V_{in} \cdot G_f \cdot \left( \frac{T \cdot r}{2JG} \right) \quad (5)$$

Substituting the known values:

$$V_{out} = 5 \cdot 2 \cdot \left( \frac{T \cdot 0.0085}{2 \cdot 3.77 \times 10^{-9} \cdot 80 \times 10^9} \right) \quad (6)$$

$$= 10 \cdot \left( \frac{T \cdot 0.0085}{6.032} \right) = T \cdot 0.000065 \quad (7)$$

### Theoretical Sensitivity

$\text{Sensitivity}_{\text{theoretical}} = 64.7 \mu\text{V/N.m}$

(8)

Thus, the theoretical sensitivity of the torque sensor is approximately  $64.7 \mu\text{V}$  per newton-meter of applied torque.

## 12 Microcontroller Programming and Communication Setup

To program the DA14531MOD Bluetooth Low Energy (BLE) microcontroller module used in our torque sensor system, we employed a structured workflow involving two primary software tools: **Keil MDK** and the **SmartBond Flash Programmer**.

**Keil MDK** (Microcontroller Development Kit) served as our integrated development environment (IDE) for firmware development. It provided a comprehensive environment for writing, compiling, and debugging embedded C code. Within Keil, we configured the project using the DA14531 Software Development Kit (SDK), selected the correct target device, and generated the corresponding firmware in the form of a .hex file. This hex file contains the binary representation of the compiled code, suitable for flashing into the microcontroller's non-volatile memory.

Once the firmware was compiled, we used the **SmartBond Flash Programmer** provided by Renesas to upload the code into the DA14531MOD's onboard SPI flash memory. This graphical tool allows easy selection of the appropriate binary or hex file and handles the low-level communication protocols required for flash programming. We connected the module to the PC via the UART or JTAG interface as specified in the module documentation, and ensured that the proper GPIO pins were configured for flashing.

After successful programming, the microcontroller executes the uploaded firmware from its flash memory and begins operation. In our setup, the DA14531MOD communicates with an external device (which runs our sensor data visualization software) via Bluetooth Low Energy. The firmware includes BLE stack initialization and characteristic definitions that allow the external application to receive real-time sensor readings wirelessly. The communication is event-driven and adheres to the GATT (Generic Attribute Profile) standard.

Figure ?? illustrates the complete workflow from development to deployment. Figure ?? depicts the BLE communication architecture between the DA14531MOD and the external device.

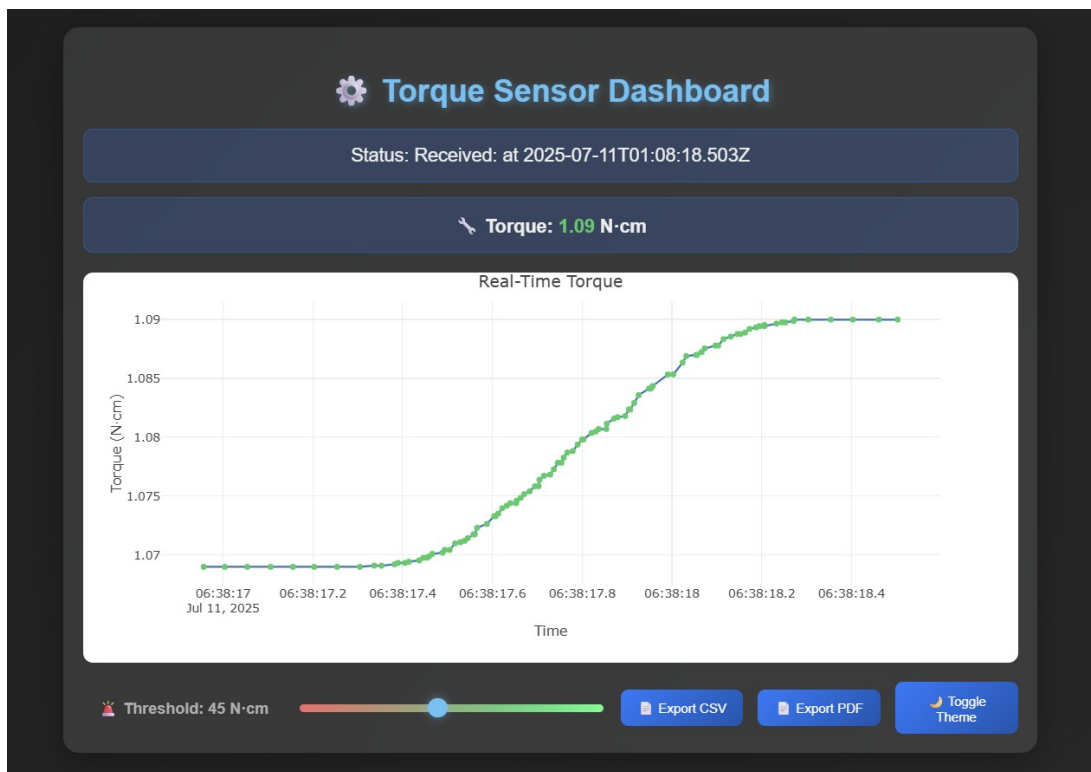


Figure 36: Software Readings

## 12.1 GPIO Reservation and Pad Configuration

The embedded firmware reserves and configures the necessary GPIO pins at initialization to ensure correct interfacing with peripheral devices such as the HX711 module, UART, LED indicators, and the SPI flash. This is done through two main functions: `GPIO_reservations()` and `set_pad_functions()`.

In development mode, `GPIO_reservations()` ensures that the required GPIO pins (e.g., HX711 DOUT and SCK) are exclusively allocated to their intended peripheral functions. This prevents resource conflicts in the system and enables clear hardware abstraction.

The `set_pad_functions()` function is then used to configure the electrical behavior of each pin (e.g., input with pull-up, output, or peripheral function). This setup enables reliable communication with the HX711, prevents unintended SPI wake-up events, and initializes the LED and UART interfaces where applicable.

Key features of the configuration:

- Ensures exclusive GPIO allocation for each hardware function.
- Uses pull-up configuration for HX711 DOUT to maintain high logic level when idle.
- Disables spontaneous wake-up from SPI Flash by setting the SPI enable pin appropriately.
- Enables LED status indication and optional UART debugging.

```
1 #if DEVELOPMENT_DEBUG
2
3 void GPIO_reservations(void)
4 {
5     RESERVE_GPIO(HX711_DOUT, HX711_DOUT_PORT, HX711_DOUT_PIN, PID_GPIO);
6     RESERVE_GPIO(HX711_SCK, HX711_SCK_PORT, HX711_SCK_PIN, PID_GPIO);
7
8 #if defined (CFG_PRINTF_UART2)
9     RESERVE_GPIO(UART2_TX, UART2_TX_PORT, UART2_TX_PIN, PID_UART2_TX);
10 #endif
11
12     RESERVE_GPIO(LED, GPIO_LED_PORT, GPIO_LED_PIN, PID_GPIO);
13
14 #if !_DA14586_
15     RESERVE_GPIO(SPI_EN, SPI_EN_PORT, SPI_EN_PIN, PID_SPI_EN);
16 #endif
17 }
18
19#endif
20
21 void set_pad_functions(void)
22 {
23     GPIO_ConfigurePin(HX711_DOUT_PORT, HX711_DOUT_PIN, INPUT_PULLUP, PID_GPIO,
24                         false);
25     GPIO_ConfigurePin(HX711_SCK_PORT, HX711_SCK_PIN, OUTPUT, PID_GPIO, false);
26
27 #if defined (_DA14586_)
28     GPIO_ConfigurePin(GPIO_PORT_2, GPIO_PIN_3, OUTPUT, PID_GPIO, true); // SPI
29                         wake-up protection
30 #else
31     GPIO_ConfigurePin(SPI_EN_PORT, SPI_EN_PIN, OUTPUT, PID_SPI_EN, true); // SPI
32                         wake-up protection
33 #endif
34
35 #if defined (CFG_PRINTF_UART2)
36     GPIO_ConfigurePin(UART2_TX_PORT, UART2_TX_PIN, OUTPUT, PID_UART2_TX, false);
37 #endif
```

```

36     GPIO_ConfigurePin(GPIO_LED_PORT, GPIO_LED_PIN, OUTPUT, PID_GPIO, false);
37 }
```

Listing 1: GPIO Reservation and Pad Configuration

## 12.2 HX711 Data Acquisition and BLE Transmission

To acquire real-time torque measurements, the system uses an HX711 24-bit ADC module to read the differential signal from the Wheatstone bridge. The data acquisition and communication to the mobile application are handled in firmware using the Dialog SDK.

The function `hx711_read()` reads the 24-bit value from the HX711, waits for data readiness, and performs a signed conversion. A timer-based callback function, `app_adcval1_timer_cb_handler()`, periodically reads this value, updates a global variable, and sends the result over BLE using a GATT notification.

The HX711 reading is converted to big-endian format before being written to the GATT database and sent to the UI. This allows seamless communication between the sensor hardware and the mobile user interface for real-time monitoring.

Key features of the implementation include:

- Timeout mechanism to avoid blocking in case of data unavailability.
- Byte-swapping for endian compatibility with mobile platforms.
- Use of `app_easy_timer()` to schedule periodic readings.
- Efficient GATT notification via `KE_MSG_ALLOC_DYN()` and `KE_MSG_SEND()`.

```

1 int32_t hx711_read(void)
2 {
3     int32_t value = 0;
4     int i;
5     uint32_t timeout = 100;
6
7     GPIO_SetInactive(HX711_SCK_PORT, HX711_SCK_PIN);
8     while (GPIO_GetPinStatus(HX711_DOUT_PORT, HX711_DOUT_PIN))
9     {
10         if (timeout == 0)
11             return 1;
12         timeout--;
13         arch_asm_delay_us(10000);
14     }
15
16     for (i = 0; i < 24; i++)
17     {
18         GPIO_SetActive(HX711_SCK_PORT, HX711_SCK_PIN);
19         arch_asm_delay_us(5);
20         value = value << 1;
21         GPIO_SetInactive(HX711_SCK_PORT, HX711_SCK_PIN);
22         arch_asm_delay_us(5);
23         if (GPIO_GetPinStatus(HX711_DOUT_PORT, HX711_DOUT_PIN))
24             value++;
25     }
26
27     GPIO_SetActive(HX711_SCK_PORT, HX711_SCK_PIN);
28     arch_asm_delay_us(5);
29     GPIO_SetInactive(HX711_SCK_PORT, HX711_SCK_PIN);
30
31     if (value & 0x800000)
```

```

32     value |= 0xFF000000;
33
34     return value;
35 }
36
37 void app_adcval1_timer_cb_handler()
38 {
39     static ke_msg_id_t adc_timer = EASY_TIMER_INVALID_TIMER;
40
41     struct custs1_val_ntf_ind_req *req = KE_MSG_ALLOC_DYN(CUSTS1_VAL_NTF_REQ,
42         prf_get_task_from_id(TASK_ID_CUSTS1),
43         TASK_APP,
44         custs1_val_ntf_ind_req,
45         DEF_SVC1_ADC_VAL_1_CHAR_LEN);
46
47     int32_t hx_val = hx711_read();
48     if (hx_val == 0)
49     {
50         KE_MSG_FREE((struct ke_msg *)req);
51         return;
52     }
53
54     adc_val_1 = hx_val;
55     req->handle = SVC1_IDX_ADC_VAL_1_VAL;
56     req->length = DEF_SVC1_ADC_VAL_1_CHAR_LEN;
57     req->notification = true;
58
59     uint32_t big_endian_val = __builtin_bswap32(adc_val_1);
60     memcpy(req->value, &big_endian_val, DEF_SVC1_ADC_VAL_1_CHAR_LEN);
61
62     attmdb_att_set_value(SVC1_IDX_ADC_VAL_1_VAL, DEF_SVC1_ADC_VAL_1_CHAR_LEN, 0,
63         (uint8_t *)&big_endian_val);
64
65     KE_MSG_SEND(req);
66
67     if (ke_state_get(TASK_APP) == APP_CONNECTED)
68     {
69         adc_timer = app_easy_timer(APP_PERIPHERAL_CTRL_TIMER_DELAY,
70             app_adcval1_timer_cb_handler);
71     }
72     else
73     {
74         adc_timer = EASY_TIMER_INVALID_TIMER;
75     }
76 }
```

Listing 2: HX711 Reading and BLE Transmission Code

## 13 Design Revisions and Improvements

### 13.1 Instrumentation amplifier

However, after further design considerations, we decided to switch to the INA333. The key reason for this change was the need for adjustable gain, which the INA333 offers via a single external resistor. This feature provides critical flexibility to tune the amplification according to the exact output of the strain gauge bridge and the input range of the ADC, allowing for better optimization of system performance.

## 13.2 Secondary Amplifier

Following a discussion with an industry expert, we identified that a secondary amplifier is not necessary in the circuit, as sufficient amplification is already provided by the ADC.

## 13.3 Offset Circuit for Instrumentation — Switching to OPA336 for instrumentation amplifier

During the design phase, various operational amplifiers were evaluated for buffering the DAC output in the offset control circuit. After a detailed analysis of their characteristics, we decided to **switch to the OPA336** for this purpose due to its superior performance in precision signal conditioning.

The key reasons for this decision are:

- **Ultra-Low Offset Voltage:** With a typical offset voltage of only  $10 \mu\text{V}$ , the OPA336 enables highly accurate offset injection, minimizing baseline error in the amplified signal.
- **Rail-to-Rail Output:** This feature allows the DAC output to fully utilize the available voltage range, ensuring effective offset tuning across the entire ADC input span.
- **Excellent Thermal Stability:** Its low input offset drift over temperature helps maintain offset accuracy even under varying environmental conditions.
- **Low Power Operation:** The OPA336 is optimized for low current consumption, making it suitable for compact and power-efficient systems like our sensor unit.
- **High Input Impedance and Low Bias Current:** These features ensure that the DAC output is not loaded, preserving the integrity of the programmed offset voltage.

**Due to these advantages, we switched to the OPA336** as the offset buffer amplifier in place of initially considered alternatives. This change enhanced the precision and reliability of the offset control in our strain gauge-based torque sensor, while also simplifying the analog front-end by eliminating the need for a separate secondary amplification stage.

## 13.4 Fabricated Enclosure

Initially, the enclosure for the product was intended to be fabricated using 3D printing techniques, primarily for rapid prototyping and ease of design iteration. However, after evaluating the requirements of the target operational environment—particularly durability, thermal resistance, and long-term mechanical stability—the decision was made to switch to a stainless steel enclosure for the final design.

This change was driven by several justifications:

- **Mechanical Strength and Durability:** Stainless steel offers significantly higher structural strength compared to typical 3D printing materials such as PLA or ABS. This ensures the enclosure can withstand external mechanical stresses and vibration in demanding industrial settings.
- **Corrosion Resistance:** Stainless steel is naturally resistant to rust and corrosion, making it suitable for long-term use in both indoor and outdoor environments, including those with moisture, dust, or chemicals.
- **Improved Heat Dissipation:** Unlike many plastic-based 3D-printed enclosures, stainless steel can efficiently dissipate heat generated by internal components, which is critical for the reliability of sensitive electronics.

- Enhanced Shielding: The metallic enclosure also provides better electromagnetic shielding, helping to minimize interference with the wireless receiver coil and other sensitive analog components.
- The finalized enclosure, fabricated from stainless steel, closely follows the original CAD design while incorporating practical features suited for real-world application. The enclosure consists of two main welded halves that are joined using bolts. The external housing provides a rigid and corrosion-resistant shell, suitable for harsh industrial environments. The interior of the enclosure includes precision-machined grooves for bearing placement, as well as welded brackets and mounts to secure the internal PCBs and wireless receiver coil.
- The structural integrity is reinforced through carefully placed welds and alignment features, ensuring a vibration-free mounting of the shaft and minimal signal distortion from mechanical noise. Furthermore, the modular design allows for straightforward disassembly and servicing, which is especially beneficial for recalibration or component replacement.

### 13.5 Transmitter PCB

During the development phase, we encountered spatial constraints with the transmitter PCB when attempting to integrate it into the enclosure. The original design did not align well with the enclosure's internal layout, making mounting and stability challenging. To address this, we redesigned the transmitter PCB to include strategically placed mounting holes at its center. This modification allowed the PCB to be securely mounted within the enclosure, ensuring proper alignment and mechanical stability, while also simplifying the assembly process. The revised design significantly improved the compactness and robustness of the final product.

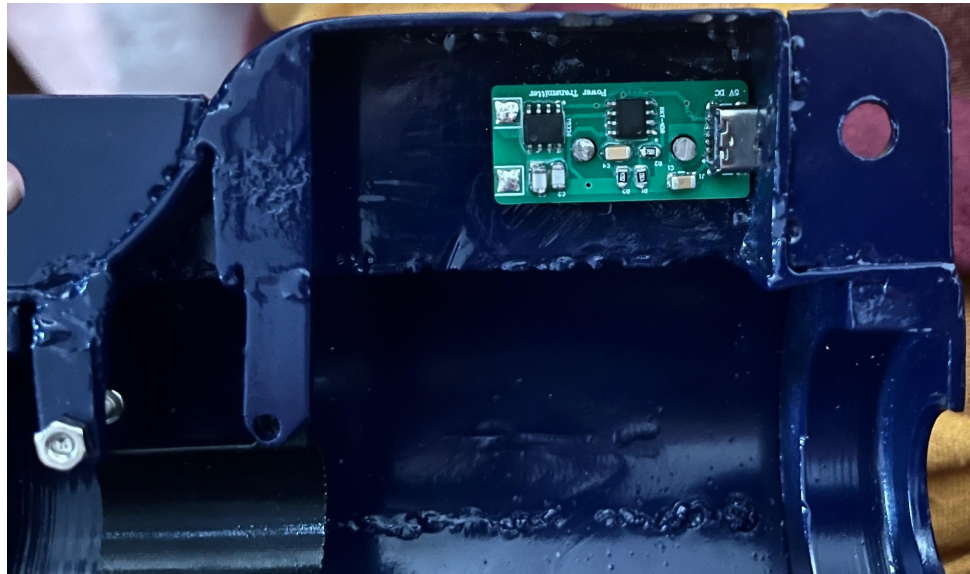


Figure 37: Transmitter PCB mounted

## 14 Bill of materials and cost analysis

Category	Item	Links	Qty	Unit Price (\$)	Total (\$)	Total (LKR)
Mechanical	Shaft Material					1,400.00
	Bearings, couplers and Bolts	Bearings				4,680.00
Sensing	Strain Gauge - SGT-2DC/350-SY11 (Omega)	Strain gauge	1	179.00	179.00	53,753.70
Signal Conditioning	Instrumentation amp	amplifier	2	5.12	10.24	3,075.072
	OPA336NA	Offset	2	2.44	4.88	1,465.464
Power	Testing					6,870.00
	Components					18,710.39
Data Acquisition	ADC	ADC	5	0.48	2.40	720.72
	Dev Board	DEV board	2	40.01	80.02	24,030.006
	MCU	MCU	2	5.86	11.72	3,519.516
PCB	Main+transmitter_1					15,000.00
	Transmitter_2					3,558.00
Enclosure						18,000.00
Components						76,829.47
Miscellaneous	Painting, paint materials, and enclosure finishing					7,430.00
	BLE DEV kit USB		2	38.75	77.50	23,273.25
						<b>Total</b> <b>262,315.59</b>

## 15 Conclusion

Through this project, we learned how to solve real-world engineering problems by combining practical design thinking with advanced technology. One of the biggest challenges was powering electronic components on a rotating shaft, which we overcame by studying and applying wireless power transfer methods used in modern devices like smartphones. This experience helped us understand how to research existing technologies, adapt them to our needs, and design a working system step by step. Overall, the project improved our skills in problem-solving, circuit design, and system integration.



Figure 38: Final View of Enclosure

## 16 References

- OPA336: OPA336 Datasheet (Texas Instruments)
- AD8293G160: AD8293 Datasheet (Analog Devices)
- DA14531: DA14531 Datasheet (Renesas)
- nRF52810: nRF52810 Product Page (Nordic Semiconductor) - Datasheet link available here
- nRF52832: nRF52832 Product Page (Nordic Semiconductor) - Datasheet link available here
- ESP32-C3: ESP32-C3 Datasheet (Espressif Systems)
- HX711: HX711 Datasheet

- LORD Torque Sensor (Reference Product): Torque Link - 200 User Manual (Microstrain)